THE ASTROPHYSICAL JOURNAL SUPPLEMENT SERIES, 79:255–284, 1992 April

A SPECTROPHOTOMETRIC ATLAS OF GALAXIES

ROBERT C. KENNICUTT, JR.
Steward Observatory, University of Arizona, Tucson, AZ 85721
Received 1991 July 29; accepted 1991 September 11

ABSTRACT

Integrated spectra of 55 nearby normal and peculiar galaxies have been compiled into a spectrophotometric atlas. Most observations cover the spectral range 3650–7100 Å, with a resolution of 5–8 Å, and sufficient signal-to-noise ratio to measure the prominent emission and absorption features. The spectra have been reduced to a common spectrophotometric scale and are presented as a series of plots, arranged according to morphological and spectral types. A digital version of the data is also available. The general characteristics of the integrated spectra of galaxies are discussed.

Subject headings: atlases — galaxies: photometry — galaxies: stellar content — techniques: spectroscopic

1. INTRODUCTION

The integrated spectrum of a galaxy is a powerful diagnostic of its stellar content and evolutionary properties. Early observations by Hubble (1926) and Humason (1931, 1936) provided some of the first systematic information on the integrated spectra of nearby galaxies, and this approach was systematized in the famous series of papers by Morgan & Mayall (1957), Morgan (1959), and Morgan & Osterbrock (1959). Today integrated spectra provide our primary source of information on the properties of very distant galaxies (e.g., reviews by Dressler & Gunn 1990 and Ellis 1990), but relatively few comparable observations are available for nearby galaxies (Wells 1972; Dressler & Gunn 1982; Gallagher, Bushouse, & Hunter 1989; Silva 1991). While abundant data on the spectra of the nuclear regions of nearby galaxies are available, these cannot be directly compared to the observations of more distant galaxies, which are made with projected aperture sizes of several kiloparsecs or more.

To address this problem I have obtained truly integrated spectrophotometry for a large and diverse sample of nearby galaxies. The main goals of this survey are to measure the systematic behavior of the nebular emission lines in galaxy spectra, as diagnostics of their star formation rates and ionization mechanisms, and to compare the properties of this nearby sample with published data for high-redshift systems. The first results of this analysis, including emission-line measurements for 80 spiral, irregular, and peculiar galaxies, are presented in Kennicutt (1992, hereafter Paper I).

During the course of this study it became apparent that high-quality spectra, with sufficient resolution and signal-to-noise ratio to isolate the primary stellar absorption features, would be a valuable resource for other applications, including the spectroscopic classification of high-redshift galaxies, spectroscopic identification of objects detected in radio, infrared, and X-ray surveys, and a variety of rudimentary spectral synthesis applications. The data from this survey reveal a rich variety of spectral properties among nearby galaxies, which cannot be adequately represented by the fragmentary data which are available in the literature. Consequently I have compiled the best spectra from the survey into this spectrophotometric atlas of galaxies.

The main part of this paper is a set of figures which display spectra of 55 normal and peculiar galaxies over the 3650–7100 Å range, most at resolutions of 5–8 Å, and grouped according to morphological and spectroscopic types (§ 3). Each figure is accompanied by a brief discussion of the general spectral properties of the individual galaxies, and the main trends which are observed along the Hubble sequence and between the different types of peculiar galaxies. Most of the discussion in this paper is qualitative, with quantitative analyses deferred to Paper I and future papers. Other parts of the paper discuss the observations, reductions, and spectrophotometric accuracy of the data (§ 2), and how a digital version of the data may be obtained (§ 3.5).

2. OBSERVATIONS

The survey was carried out in two stages. Large-aperture, moderate-resolution (15–25 Å) spectrophotometry was obtained for 70 galaxies in 1985–1987, using the Intensified Reticon Scanner (IRS) on the 0.92 m telescope at Kitt Peak National Observatory (KPNO). This provided continuum energy distributions and emission-line fluxes for a large set of galaxies, but the spectral resolution of these data was insufficient for accurate measurements of weak absorption or emission features. Subsequently higher resolution (5–7 Å) data were obtained for 44 galaxies in 1989–1991, using a long-slit drift scanning technique on the Steward Observatory 2.3 m telescope.

2.1. *High-Resolution Spectra*

Most of the spectra in this atlas were obtained with the Boller & Chivens (B&C) Spectrograph on the Steward Observatory 2.3 m telescope. In order to observe very large galaxies (D = 1′–14′) while maintaining high spectral resolution, a narrow long slit was used, and the galaxy images were trailed across a

[1] Visiting Astronomer, Kitt Peak National Observatory, National Optical Astronomical Observatories, which are operated by the Association of Universities for Research in Astronomy, Inc. (AURA), under cooperative agreement with the National Science Foundation.

long slit several times during each integration. The spectral resolution was dictated by the slit width, while the aperture on the sky was defined by the lengths of the slit and the drift scan. A total of 44 galaxies were observed with this setup, and spectra for 41 of these are included in the atlas.

The B&C spectrograph was used with a thinned 800 × 800 TI CCD, which was UV-flooded for enhanced blue response. Two grating settings were used to cover the full visible spectrum. A 600 gpm grating blazed at 3568 Å covered the 3650–5150 Å region, and a 400 gpm grating blazed at 7500 Å (with 4200 Å blocking filter) covered the 4950–7150 Å region. A 2″.5 slit yielded a resolution of 4.5 Å in the blue and 7 Å in the red. The usable slit length for the observations was approximately 3′.5; galaxies with diameters along the slit of ≤2′.5 were observed, in order to provide adequate coverage for sky subtraction. Several larger, inclined galaxies were measured by aligning the slit with the minor axis, and drift scanning the telescope along the major axis. The scan lengths were 45″–800″, and the drift rates were adjusted so that the image crossed the slit at least 4 times, to minimize errors due to small variations in drift speed or transparency. Integration times were 20–60 minutes. Shot noise from the sky background dominated over CCD readout noise in all cases.

Each CCD observation contained 130 pixels (1″.6 after binning) along the slit. Since the telescope was drifted during the exposure, however, each pixel of this two-dimensional spectrum actually is a line integral of the luminosity distribution, averaged along the scan direction, and most direct spatial information is lost. Consequently the data were summed along the slit into one or more one-dimensional sky-subtracted spectra. Each of these is equivalent to a fixed observation with a rectangular aperture, with dimensions set by the length of the drift scan in one direction, and the summation limits (along the slit) in the perpendicular direction. The aperture limits were selected to contain most of the integrated luminosity of the galaxies (A/D_{25} = 0.5–1), while excluding contamination from bright foreground stars. Although all parts of the galaxy within the aperture were weighted equally in the integrated spectrum, the very faint outer regions ($\mu_B \sim 24$ and fainter) were often excluded from the aperture. Comparisons of spectra extracted with different size apertures indicates that the data here closely approximate the integrated spectra, but the slight undersampling may influence the interpretation of the data for some applications.

Data reduction followed standard techniques, using the IRAF software package. Special care was taken in the flat-field response calibration and cosmic-ray removal, steps necessitated by the low surface brightness of the galaxies when observed in drift-scanned mode. Separate dome and sky flat-field exposures were obtained, and regions which deviated by more than 1% (~0.3% after a linear fit along the slit) were discarded. Cosmic-ray events were removed in two steps, first with an automated sigma-rejection routine, followed by removal of residual events by hand.

One-dimensional spectra for the galaxies were extracted interactively, by using the observed intensity profile along the slit to define the apertures and sky background regions. The spectrophotometry was calibrated using observations of standard stars from Massey et al. (1988). Stars were observed in fixed pointings, with the slit oriented along the direction of atmospheric dispersion. The blue and red spectra were tied together by normalizing the mean continuum intensities in the 4950–5150 Å overlap region, or in the [O III] λ5007 emission line. Errors of ~5% in the flux scale between regions shortward and longward of 5100 Å are possible. This level of uncertainty is unimportant for all of the applications in this paper, but it may be an important consideration for applications which require the continuum shape to be accurately determined. The overall accuracy of the spectrophotometry is discussed in detail in § 2.3.

2.2. *Low-Resolution Spectra*

Spectra covering the range 3650–6900 Å were obtained for 70 galaxies during three observing runs in 1987–1989, using the IRS spectrometer on the KPNO No. 2 0.92 m telescope (f/7.5 focus). The lower resolution of these data (10–25 Å) makes them less useful for general applications, but spectra for 14 galaxies, mostly strong emission-line galaxies, are included in the atlas.

The IRS is a dual-beam spectrometer, with an unusual combination of a compact image scale and fast camera, which make it possible to obtain moderate-resolution spectra with large entrance apertures. All of the observations reported here are fixed pointed measurements, made with a pair of 45″.5 circular apertures, with centers separated by 61″.2 on an east-west line. The galaxies were observed using a 500 gpm grating blazed at 5500 Å with a WG-360 UV-blocking filter, which provided photometric coverage over 3700–6900 Å. With the large apertures, the spectral resolution was modulated by the luminosity distributions of the galaxies, ranging from 12 Å FWHM for a point source (such as an emission line nucleus) to 25 Å for uniform illumination of the 45″ apertures. The actual resolution for most of the data is 15–20 Å FWHM. Additional observations in the blue (3600–5500 Å) were obtained for approximately half of the program galaxies, using a 400 gpm grating blazed at 8000 Å in second order behind a $CuSO_4$ filter. This provided somewhat better resolution (typically 9–13 Å), and higher sensitivity shortward of 4000 Å. Most of the spectra shown here are the low-dispersion observations, but in a few cases (Mrk 158, Mrk 201, NGC 3303) the low- and intermediate-dispersion data were combined to improve the signal-to-noise ratio in the blue.

Each observation consisted of a series of integrations in alternating apertures, with the beam-switching performed under computer control. Total integration times were 4–180 minutes, depending on the brightness of the galaxy and the relative strengths of the emission lines. The data were taken in photometric or near-photometric conditions.

True integrated spectra were only obtained for galaxies with diameters less than 45″, including most of the emission-line galaxies shown here. A few of the galaxies have diameters considerably larger than the aperture, and the spectrum shown refers to the central 45″ region. For a few very large galaxies, including one published here (NGC 5866), observations were made in nebular mode, i.e., with both apertures on the object, alternated with pairs of sky observations. Observations at three positions (pairs) were combined to yield a pseudo-integrated spectrum.

The spectra were calibrated using observations of HeNeAr and quartz lamps, and spectrophotometric standards from the

IRS standard star catalog. Data reductions followed standard techniques, using the on-line mountain programs for flat-fielding and wavelength calibration, and the spectral reduction programs within the IRAF package for flux calibration. Special care was taken to check the accuracy of the large-aperture spectrophotometry. The uniformity in spectral response over the large apertures was checked by dividing flat-field exposures obtained with different aperture sizes, and by observing a standard star placed at various positions within the large aperture. These tests confirmed that the spectral response using the 45″ apertures matched that obtained with smaller apertures at the 1% level. Probably the most important source of systematic error is a small level of crosstalk between the two reticon channels, caused by scattered light in the IRS (Barnes, Massey, & Carder 1986), which may introduce errors of several percent in the energy distributions, as discussed below.

2.3. *Spectrophotometric Accuracy*

The photometric errors in these spectra are dominated by uncertainties in the spectrophotometric calibration, flatfielding, and sky subtraction. Typical residuals of individual standard stars from the mean calibration were a few percent or less, but the galaxy spectra, derived with much larger apertures, are less precise. Several tests were made to assess the reliability of the data.

As an external check on the spectrophotometry, a mean spectrum was computed for the elliptical galaxies observed with each instrument, and compared with the large-aperture scanner observations by Schild & Oke (1971) and Whitford (1971). Figure 1 shows this comparison. The ordinate shows the normalized magnitude AB_ν, defined as

$$AB_\nu = -2.5 \log f_\nu + C , \quad (1)$$

where C is the flux at 5500 Å. The agreement for both telescopes is quite good, though both sets of spectra show deviations of up to 10%, especially in the red. Some of the difference may arise because different galaxies were observed; Schild & Oke (1971) found that the energy distributions of individual elliptical galaxies often differ at the 10%–20% level over this wavelength range. The internal tests discussed below, however, suggest that most of the residuals are due to uncertainties in the current observations.

Several galaxies were observed with both instruments, and intercomparison of these data provides another useful check on the spectrophotometry. Figure 2 shows a comparison of spectra of the Coma elliptical NGC 4889, observed with the 2.3 m (*solid line*) and 0.92 m (*dotted line*) telescopes. The spectra are normalized to unity at 5500 Å, and the IRS spectrum is shifted down by 0.2 for clarity. The two spectra match well, but deviations of up to ±10% are present. Similar residuals, ranging from ±7%–15%, are found for the sample as a whole, including a systematic tendency for the IRS spectra to be redder (cf. Fig. 2). Again, part of the difference may be a real aperture effect, caused by the well-known color gradients in E/S0 galaxies (e.g., Kormendy & Djorgovski 1989), but much appears to be instrumental in origin. In particular the 2.3 m spectra are subject to small errors ($\lesssim$10% level) due to wavelength-dependent atmospheric seeing, introduced because the galaxies were drift-scanned across a 2″.5 slit, whereas the standard stars were observed in fixed pointings (always with the slit oriented along the parallactic angle). According to Woolf (1982), the seeing disk at 7100 Å is roughly 12.5% smaller than at 3650 Å, and under typical seeing conditions at Kitt Peak this will introduce an artificial gradient of a few percent in the calibration of the drift-scanned galaxy observations relative to the standard stars, in the same direction as observed in Figures 1 and 2. Since the size of the effect is small and varies with the seeing itself, no attempt has been made to apply a correction.

These tests indicate that the energy distributions have typical uncertainties of ±10% peak-to-peak over large wavelength regions, with occasional errors as large as ±15%. These values represent the *maximum* errors in any given spectrum; the rms deviations averaged over the entire spectrum are usually at least 2–3 times smaller. This accuracy is adequate for most applications, but these data are not recommended for cases where precise energy distributions are crucial (e.g., computation of K-corrections, detection of low-level blue stellar populations), without a careful consideration of the limitations discussed above.

Measurements of local spectral features show excellent reproducibility, with accuracies of a few percent. Two special situations merit a brief mention, however. When absorption and emission features of comparable strength are superposed, such as with Hβ and the higher order Balmer lines, the detectability of the respective features is a very strong function of the resolution and signal-to-noise ratio of the spectrum. This is usually not a problem for the 2.3 m data, which comprise most of this atlas, but blending may affect a few of the galaxies observed with the IRS. See Paper I for a complete discussion of this effect. Another problem occasionally occurs when a spectral feature in the galaxy falls near a bright night sky line. Due to small irregularities in the flatness of the CCD detector on the 2.3 m spectrograph, which introduces slight variations in the point-spread function along the slit, subtraction of strong sky lines is never perfect, and residual features of a few percent are common. This is a problem only if the artifact falls near a real feature, such as Na D at low redshift, or Hγ near Hg λ4358. As an aid in identifying such artifacts in the galaxy spectra, a plot of the night sky spectrum (with both full and expanded scales) is shown in Figure 3.

3. THE SPECTRAL ATLAS

3.1. *Galaxy Sample*

Table 1 lists the basic properties of the galaxies in the atlas, arranged in order of presentation, along with information about the observations. Columns (1) and (2) give the galaxy name and the number of the figure or figures in which the spectrum appears, respectively. Column (3) gives the morphological type, taken (in order of precedence) from the Revised Shapley-Ames Catalog (Sandage & Tammann 1981), the Second Reference Catalog of Bright Galaxies (de Vaucouleurs, de Vaucouleurs, & Corwin 1976), Huchra (1977), or as classified by the author. Columns (4) and (5) list the redshift and corrected absolute blue magnitude, with photometry taken from the catalogs listed above, and assuming a Hubble constant $H_0 = 75$ km s^{-1} Mpc^{-1}. Column (6) gives the telescope

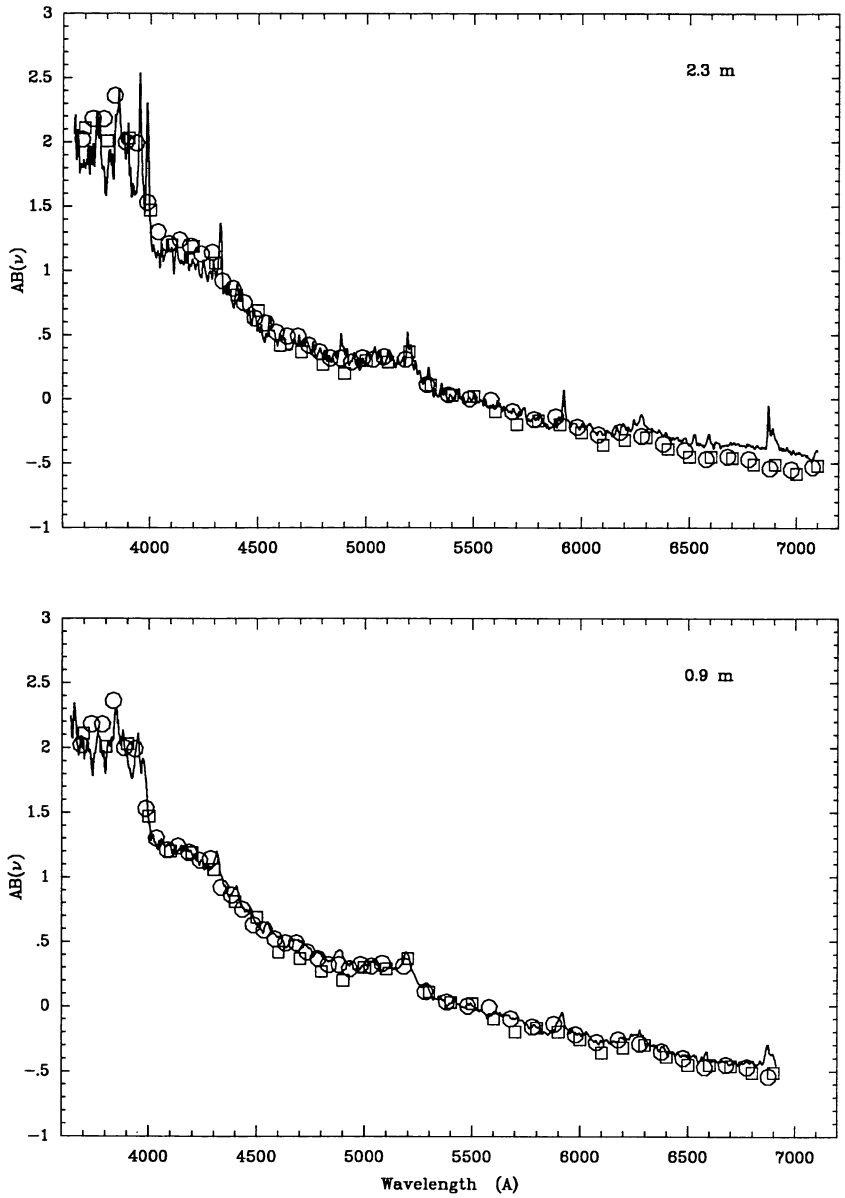

FIG. 1.—Comparison of mean spectra of giant elliptical galaxies observed here (*solid lines*) with spectrophotometric scanner observations by Schild & Oke (1971; *open squares*) and Whitford (1971; *open circles*). See text for definition of the normalized flux $AB(\nu)$.

used in the observation, and column (7) lists the aperture diameter, with a single value for a circular aperture, and two numbers for a rectangular scan (east-west by north-south). Special notes or remarks are indicated in column (8).

The atlas is divided roughly equally between normal and peculiar galaxies. Although peculiar galaxies comprise only a few percent of the local population, they appear with much higher frequency in surveys of high-redshift objects, or in surveys of radio, infrared, or X-ray luminous sources. The peculiar galaxies also possess a very large range of spectral properties, and for these reasons a considerable portion of the atlas is devoted to these objects. An effort was made to include a complete set of spectral types observed in nearby and distant galaxies. Although it is quite possible that some extremely peculiar spectral classes are missing here, I was able to find local analogs to essentially every type of spectrum observed in published surveys of high-redshift or active galaxies. More details concerning the selection criteria and sources for sample may be found in Paper I.

3.2. *Presentation of the Spectra*

The spectra for the 55 galaxies in the atlas are presented in Figures 5–22. The spectra are grouped four to a page; this represented a compromise between retaining the maximum detail while conserving space. This has the additional advantage of making it much easier to compare spectra of a given galaxy type and to see subtle differences between the spectra. The groupings were carefully selected with this in mind. For each figure an accompanying description is given in § 3.3, and I

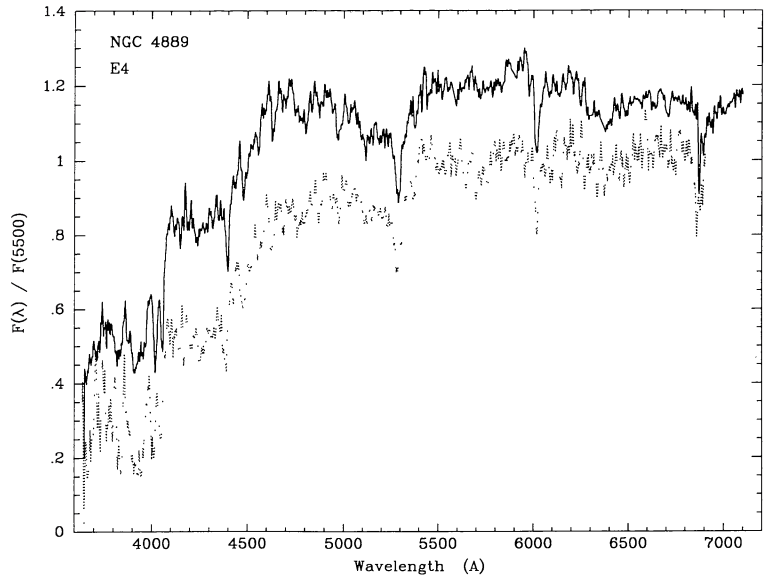

FIG. 2.—Comparison of integrated spectra of the Coma cluster giant elliptical NGC 4889, obtained by drift scans with the Steward Observatory 2.3 m telescope (*solid line*), and by large-aperture spectrophotometry on the KPNO 0.92 m telescope (*dotted line*). The spectra have been shifted by 0.2 flux units for clarity.

recommend that the reader consult this text while examining the spectra themselves.

All spectra are plotted on a common wavelength scale of 3500–7200 Å, except for Figures 12, 14, and 18, which show expanded spectra in the blue (3600–5400 Å) for selected galaxies. The intensities are plotted as flux per unit wavelength, normalized to unity at 5500 Å. The spectra have been corrected for atmospheric extinction, but have not been corrected for foreground Galactic reddening or reddening within the galaxies themselves. The vast majority of the galaxies were observed at high Galactic latitude, where foreground reddening is likely to be negligible, but there are a few exceptions, most notably NGC 1569 ($b = 11°$) in Figures 11 and 19. It is important to note that since the spectral resolution varies slightly with wavelength (and changes by a factor of 1.5 on either side of 5120 Å in the 2.3 m data), the heights of the emission lines should only be taken as a qualitative indication of the relative line strengths. Paper I contains complete listings of emission line fluxes and equivalent widths for the galaxies.

Prior to plotting, most of the spectra were rebinned in wavelength and smoothed with a 4 and 6.5 Å square filter for the 2.3 and 0.92 m data, respectively. For clarity of presentation, resid-

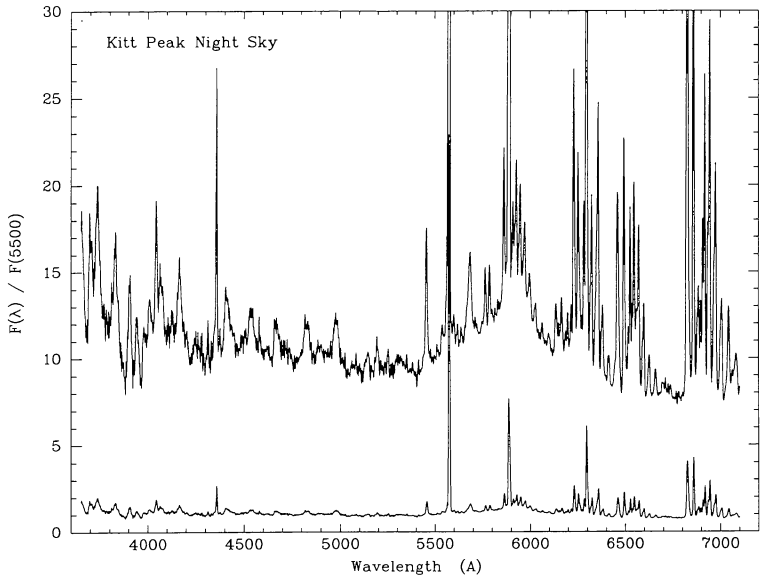

FIG. 3.—A typical night sky spectrum at Kitt Peak. The lower plot shows the full night sky spectrum, normalized to unity at 5500 Å. The top plot is the same spectrum expanded by a factor of 10 in intensity.

TABLE 1

GALAXIES IN THE ATLAS

Name (1)	Figure(s) (2)	Type (3)	cz (km s^{-1}) (4)	$M(B)$ (5)	Instrument (m) (6)	Aperture (7)	Notes (8)
NGC 3379	5	E0	760	−19.7	2.3	120 × 180	
NGC 4472	5	E1/S0	820	−21.5	0.9	45	1
NGC 4648	5	E3	1640	−19.0	2.3	60 × 60	
NGC 4889	5	E4	6480	−22.1	2.3	60 × 60	2
NGC 3245	6	S0	1210	−19.3	2.3	90 × 90	
NGC 3941	6	SB0/a	940	−19.2	2.3	90 × 90	
NGC 4262	6	SB0	1250	−18.4	2.3	90 × 90	1
NGC 5866	6	S0	820	−19.3	0.9	165 × 45	3
NGC 1357	7	Sa	2100	−20.2	2.3	120 × 90	
NGC 2775	7, 12	Sa	1200	−19.9	2.3	90 × 90	
NGC 3368	7	Sab	760	−20.5	2.3	120 × 180	
NGC 3623	7	Sa	680	−20.6	2.3	90 × 600	
NGC 1832	8	SBb	1860	−20.6	2.3	90 × 90	
NGC 3147	8	Sb	2900	−22.0	2.3	120 × 120	
NGC 3627	8	Sb	590	−19.9	2.3	150 × 180	
NGC 4750	8, 12	Sb pec	1830	−20.2	2.3	90 × 45	
NGC 2276	9	Sc	2650	−21.2	2.3	120 × 120	4
NGC 4775	9, 18	Sc	1380	−19.9	2.3	90 × 90	
NGC 5248	9	Sbc	1050	−20.3	2.3	150 × 180	
NGC 6217	9	SBbc	1600	−20.2	2.3	90 × 90	
NGC 2903	10	Sc	470	−20.1	2.3	150 × 360	
NGC 4631	10	Sc	610	−20.5	2.3	800 × 110	
NGC 6181	10	Sc	2440	−20.7	2.3	90 × 60	
NGC 6643	10, 12	Sc	1740	−20.7	2.3	120 × 90	
NGC 1569	11, 18	Sm/Im	140	−16:	2.3	120 × 60	5
NGC 4449	11, 12	Sm/Im	250	−17.9	2.3	180 × 120	6
NGC 4485	11	Sm/Im	820	−18.3	2.3	90 × 90	4
NGC 4670	11	SB pec	1040	−18.1	2.3	60 × 45	7
NGC 3034	14, 15	I0	410	−18.5	2.3	314 × 120	6, 8
NGC 3077	14, 15	I0	160	−17.1	2.3	120 × 120	
NGC 5195	14, 15	I0 pec	550	−18.8	2.3	90 × 90	4
NGC 6240	14, 15	I0 pec	7600	−21.	2.3	40 × 45	4
NGC 3310	16, 18	Sbc pec	1070	−19.9	2.3	90 × 65	
NGC 3690	16	Sc pec	3100	−21.4	0.9	45	4, 9
NGC 6052	16	Sm pec	4780	−20.8	0.9	45	4, 10
UGC 6697	16	S pec	6600	−21.	2.3	120 × 20	11
NGC 2798	17, 18	Sa pec	1770	−18.9	2.3	60 × 90	4, 12
NGC 3471	17	Sa	2140	−19.2	0.9	45	12, 13
NGC 5996	17	SBd	3310	−20.4	0.9	45	12, 14
NGC 7714	17	S pec	2970	−20.2	2.3	60 × 45	12, 15
Mrk 35	19	pec	1090	−17.6	0.9	45	16
Mrk 59	19	SBm/Im	840	−17.7	0.9	45	17
Mrk 71	19	SBm	280	−16.6	0.9	45	18
Mrk 487	19	Im	780	−14.8	0.9	45	
NGC 3516	20	S0	2840	−20.5	2.3	60 × 60	19
NGC 5548	20	Sa	4960	−21.2	2.3	60 × 45	19
NGC 7469	20	Sa	5120	−22.2	0.9	45	4, 19
NGC 3227	21	Sb	1100	−19.9	2.3	120 × 180	4, 20
NGC 6764	21	SBb	2410	−20.	0.9	45	20
Mkr 3	21	S0	4110	−20.8	2.3	60 × 45	20
Mkr 270	21	S0	2700	−19.0	2.3	60 × 45	20, 21
NGC 1275	22	E pec	5430	−22.4	2.3	75 × 60	22
NGC 3303	22	Pec	6300	−20.	0.9	45	4
NGC 3921	22	S0 pec	6020	−20.0	2.3	60 × 45	4, 23
NGC 4194	22	Sm pec	2670	−19.8	0.9	45	4, 24

NOTES.—(1) Virgo Cluster member. (2) Coma cluster member. (3) Observed in nebular mode; aperture values refer to major and minor axes. (4) Strongly interacting or merging galaxy. (5) Spectrum shape affected by high Galactic foreground reddening. (6) Drift scan oriented with major axis. (7) Haro 9. (8) M82. (9) Mrk 271. (10) Mrk 297. (11) Member of Abell 1367 cluster. (12) Starburst nucleus. (13) Mrk 158. (14) Mrk 691. (15) Mrk 538. (16) NGC 3353; Haro 3. (17) NGC 4861; aperture centered on giant H II region. (18) NGC 2366; aperture centered on giant H II region (NGC 2363). (19) Seyfert 1 nucleus. (20). Seyfert 2 nucleus. (21) NGC 5283. (22) Located in Perseus cluster; double emission-line system. (23) Mrk 430. (24) Mrk 201.

ual features from the brightest night sky lines (mainly [O I] λ5577, 6300, 6363, NaD when sufficiently isolated) have been clipped, except in cases where the lines fall near real spectral features in the galaxies. The night sky spectrum in Figure 3 can be consulted for identification of these lines. Telluric absorption features (e.g., the B band near 6870 Å) have not been removed.

As an aid to interpreting the galaxy spectra, Figure 4 reproduces spectra for 4 reference stars from the library of Jacoby, Hunter, & Christian (1984). These stars include the predominant contributors to the integrated starlight in most galaxies, and may provide a useful means of identifying many of the prominent absorption features. For more detailed comparisons I refer the reader to the Jacoby et al. (1984) paper, which presents dereddened spectra for 134 stars in the same format as given here. Nebular emission features in the galaxy spectra can be identified by comparison with Figure 19, which shows four H II galaxies.

3.3. *Description of Galaxy Spectra: Normal Galaxies*

3.3.1. *Elliptical Galaxies (Fig. 5)*

The elliptical galaxies show relatively homogeneous spectra, dominated by absorption features from cool giants. The variation in line features are mainly due to differences in metallicity and line broadening. NGC 4472 was observed at low resolution with the IRS and illustrates well the effect of reduced spectral resolution on the observed spectra. The difference in continuum slopes longward of 5500 Å between NGC 3379 and the other galaxies is probably instrumental, and this serves as a good illustration of the calibration errors discussed in § 2.3.

Nebular emission lines are absent or weak in these galaxies, as in the S0 galaxies illustrated in Figure 6. The most easily seen emission line, when present, is [O II] λ3727, which varies in equivalent width from 0 to 4 Å among the E/S0 galaxies. Approximately half of the early-type galaxies in the survey show detectable [O II] emission in the integrated spectrum. [N II] λ6583 is sometimes detected as well. The Balmer lines are almost always seen in absorption. The line emission probably originates in the nucleus in most cases or from diffuse interstellar gas (e.g., Osterbrock 1960).

3.3.2. *S0–S0/a Galaxies (Fig. 6)*

As a class the spectra of the S0 galaxies are nearly indistinguishable from those of the elliptical galaxies in Figure 5, at least within the errors of the data presented here. Even if a low-level blue continuum from young stars were present (Gregg 1989), it probably would not be detected in our data. Weak [O II] and [N II] emission is frequently observed, with equivalent widths of a few angstroms or less, similar to the elliptical galaxies discussed above. NGC 3245, 3941, and 4262 were observed with the 2.3 m telescope, while the spectrum of NGC 5866 is the sum of three pairs of nebular observations made with the 0.92 m telescope and IRS.

3.3.3. *Sa–Sab Galaxies (Figs. 7 and 12)*

Although the visible spectra of these galaxies are still dominated by evolved giant stars, additional signatures of a younger population are now evident. The most obvious is the appearance of emission lines (in decreasing order) [N II] λ6583, [O II] λ3727, Hα, and rarely Hβ or [O III] λ5007. The equivalent widths of these lines are usually only a few angstroms, and the Balmer lines, including Hα, are still strongly affected by stellar absorption. The presence of a younger population can be seen in the continuum in the blue, especially at the 4000 Å H + K break (also see Fig. 22). The absorption spectra also begin to show subtle changes (e.g., Ca II K vs. H + Hε or G band vs. Hγ), but this is not readily apparent in the plots shown here.

The Sa–Sab galaxies display a large range in spectral properties in the emission lines and in the blue continuum, which presumably reflects a range in star formation rates per unit mass or area (cf. Caldwell et al. 1991). These differences in spectra are not always correlated with their published Hubble types. For example, the spectrum of NGC 1357, an Sa galaxy (Sandage & Tammann 1981) is considerably bluer than those of NGC 3368 or NGC 488 (not shown), both classified as Sab galaxies. This illustrates how a purely spectroscopic classification would differ somewhat from a traditional morphological classification based on disk resolution, bulge/disk morphology, or spiral arm properties. Examination of the entire sample shows that such inconsistencies are common when one compares spirals within a given subtype (e.g., Sa vs. Sab) or occasionally even between adjacent types (e.g., Sb vs. Sc), but in general the sequence of stellar populations revealed by the integrated spectra show an excellent congruity with the purely morphological classifications of de Vaucouleurs et al. (1976) and Sandage & Tammann (1981).

3.3.4. *Sb Galaxies (Figs. 8 and 12)*

The presence of a mixed age stellar population is most apparent in the Sb galaxies. Nebular emission lines are now prominent features, including Hα + [N II], with equivalent widths of ~5–30 Å, and weaker emission in [N II], [S II], and [O II]. Blueward of Hα, however, [O II] is the only consistently detectable emission line. A blue continuum from young stars is readily apparent (also see Fig. 12), and the G- and K-giant–dominated absorption features begin to weaken in favor of the Balmer lines. The visible–red continuum is still dominated by late-type giants, however.

The range of spectral properties among the Sb galaxies, in both the continuum and the emission lines, is very large, reflecting the nearly tenfold variation in star formation rate per unit mass within the class (Kennicutt 1983). Again there are examples of galaxies whose stellar content do not match their morphological classification, e.g., NGC 1832, with the spectrum of a prototype Sc galaxy (see Figs. 9–10).

Perhaps the most surprising result in Figures 5–8 is the very slow progression of spectral properties (exclusive of the Hα + [N II] emission lines) between types E and Sb. Unless one were able to measure the blue continuum colors or [O II] λ3727 emission line to high accuracy, it would be difficult to distinguish the spectrum of an early- to intermediate-type spiral from an E/S0 galaxy. This point is addressed further in § 3.3.7.

3.3.5. *Sbc–Sc Galaxies (Figs. 9, 10, 12, and 18)*

Figures 9 and 10 show spectra for eight Sbc–Sc galaxies. The galaxies in Figure 9 are arranged to illustrate the variations in continuum shape and emission-line strength, while Figure 10

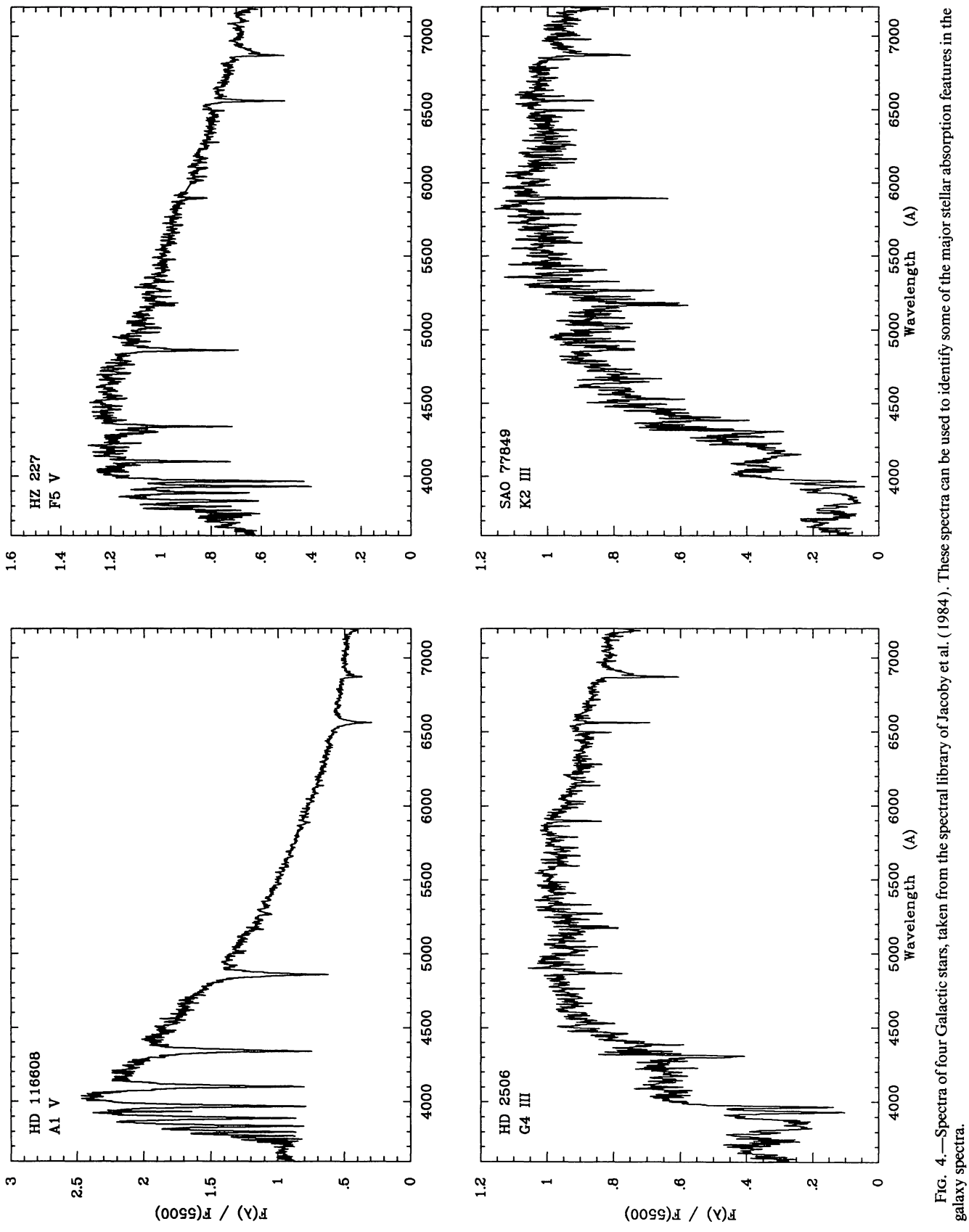

FIG. 4.—Spectra of four Galactic stars, taken from the spectral library of Jacoby et al. (1984). These spectra can be used to identify some of the major stellar absorption features in the galaxy spectra.

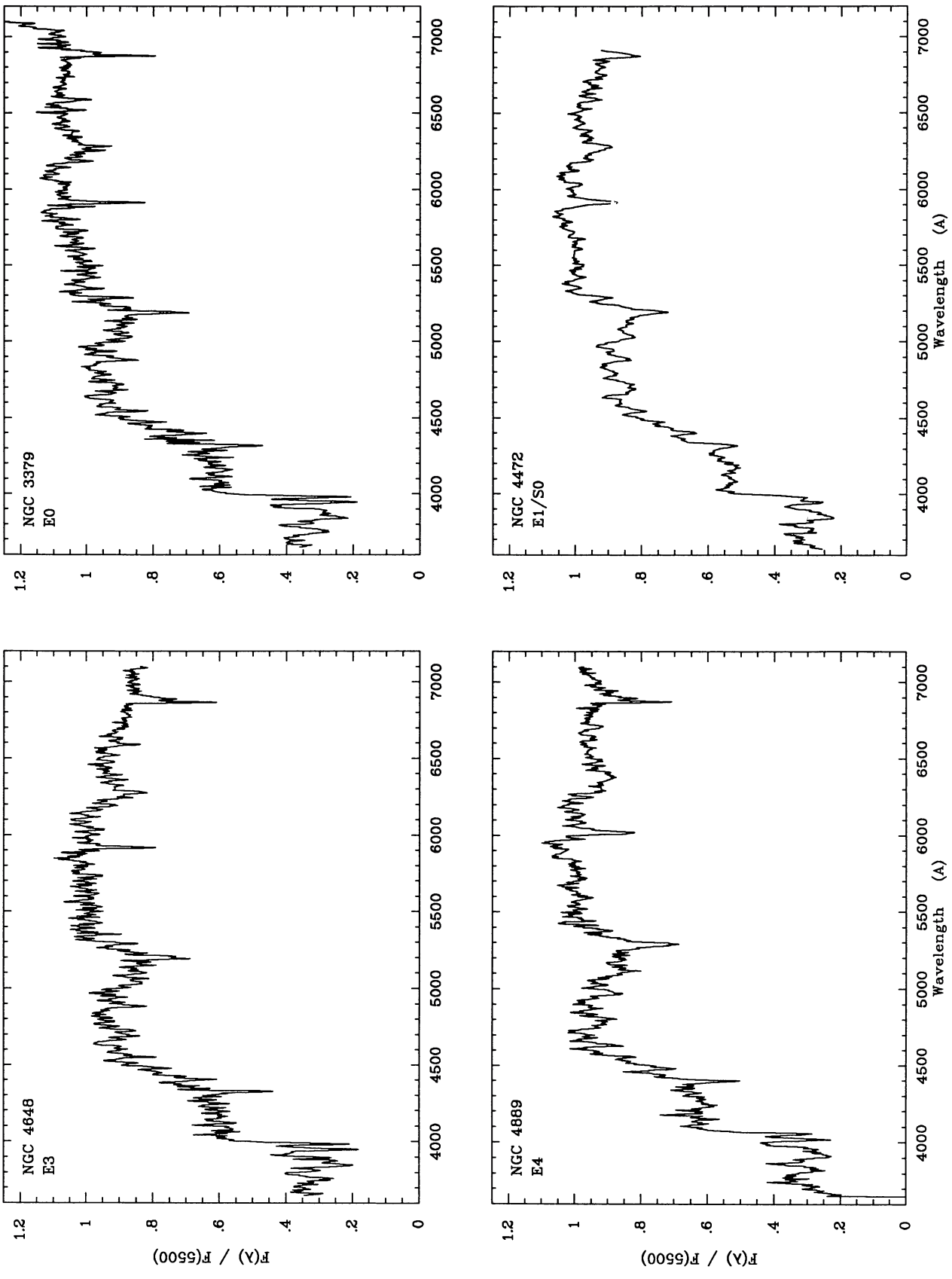

FIG. 5.—Integrated spectra of four elliptical galaxies. The spectrum of NGC 4472 (*lower right*) was obtained at lower resolution with the IRS scanner.

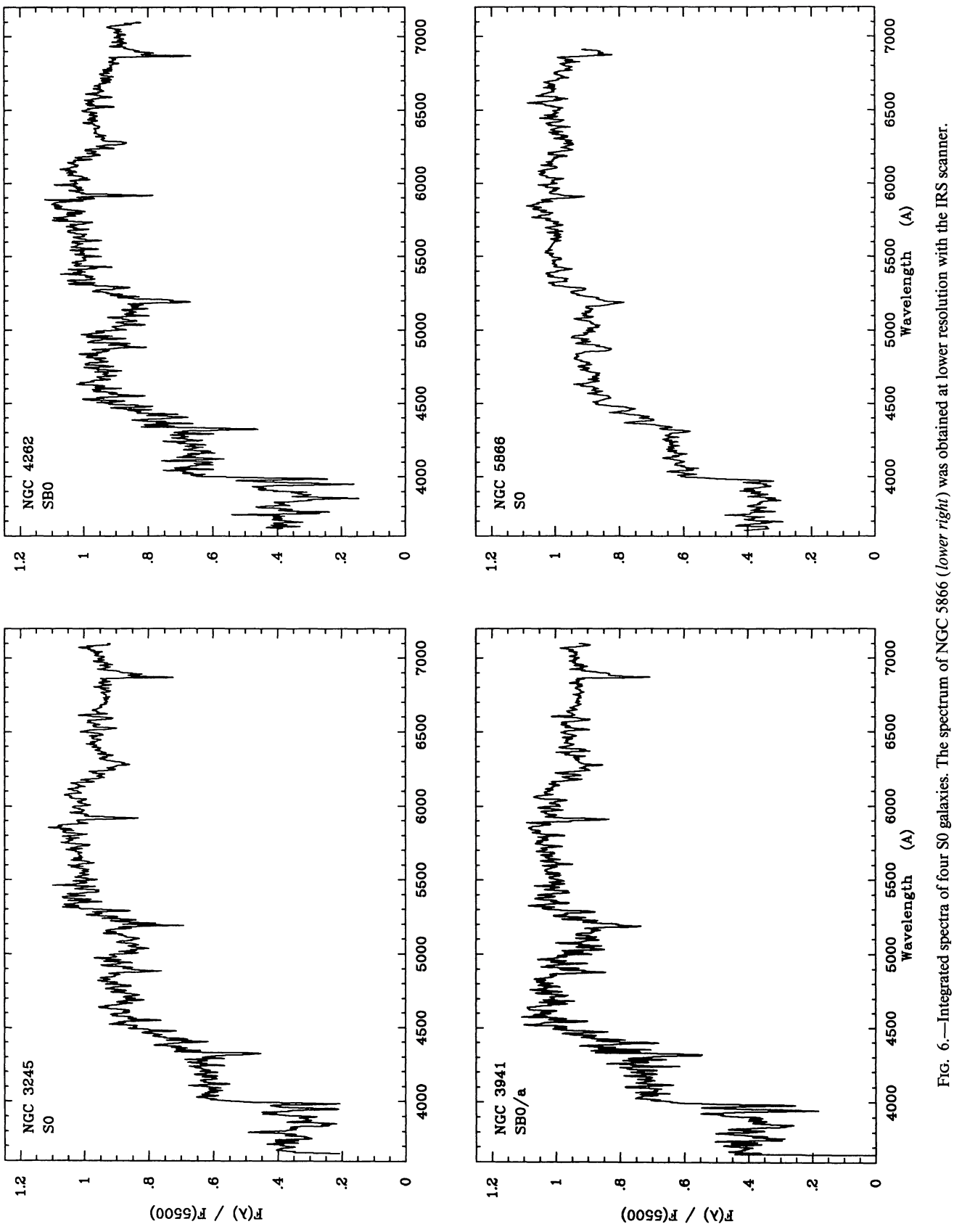

FIG. 6.—Integrated spectra of four S0 galaxies. The spectrum of NGC 5866 (*lower right*) was obtained at lower resolution with the IRS scanner.

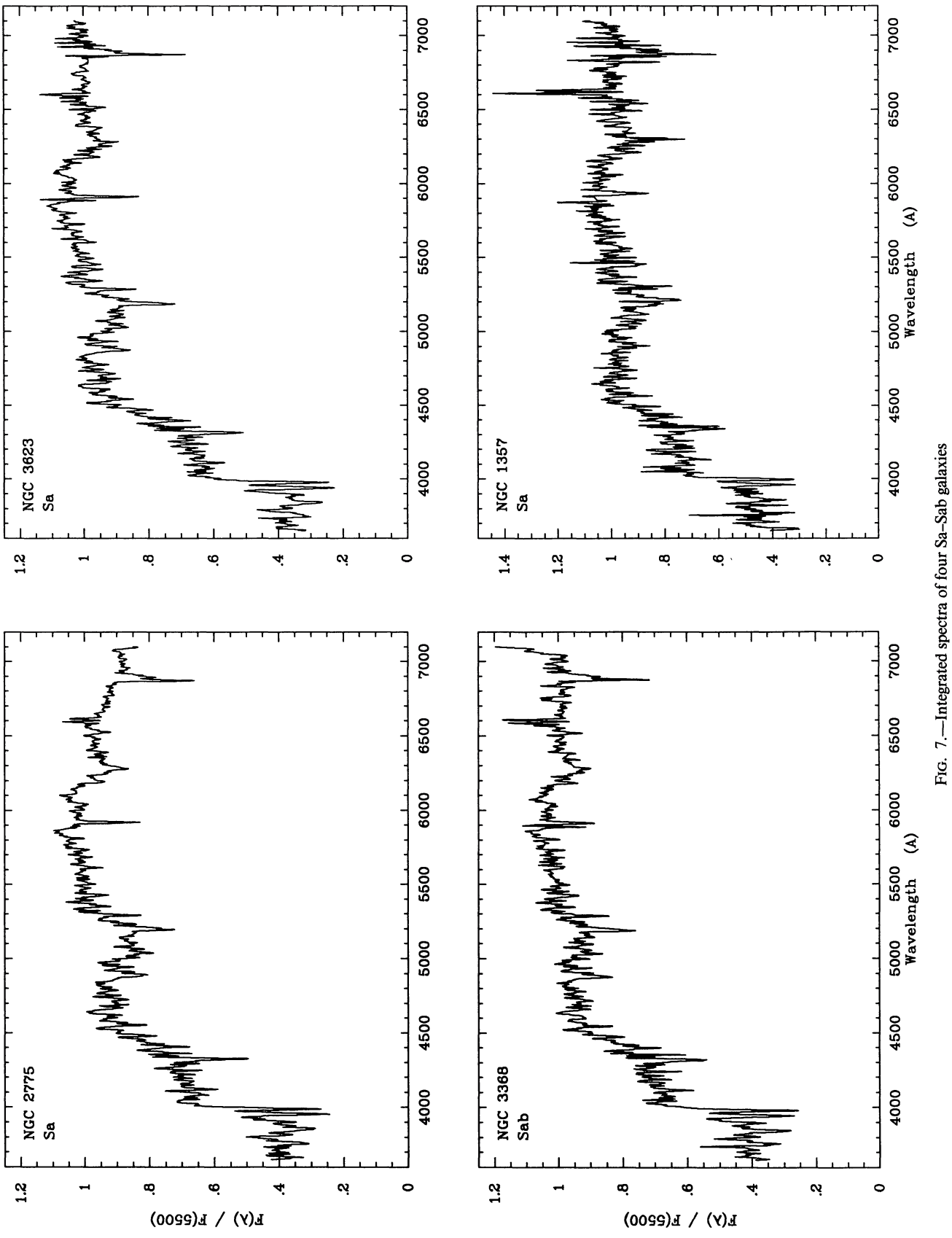

FIG. 7.—Integrated spectra of four Sa–Sab galaxies

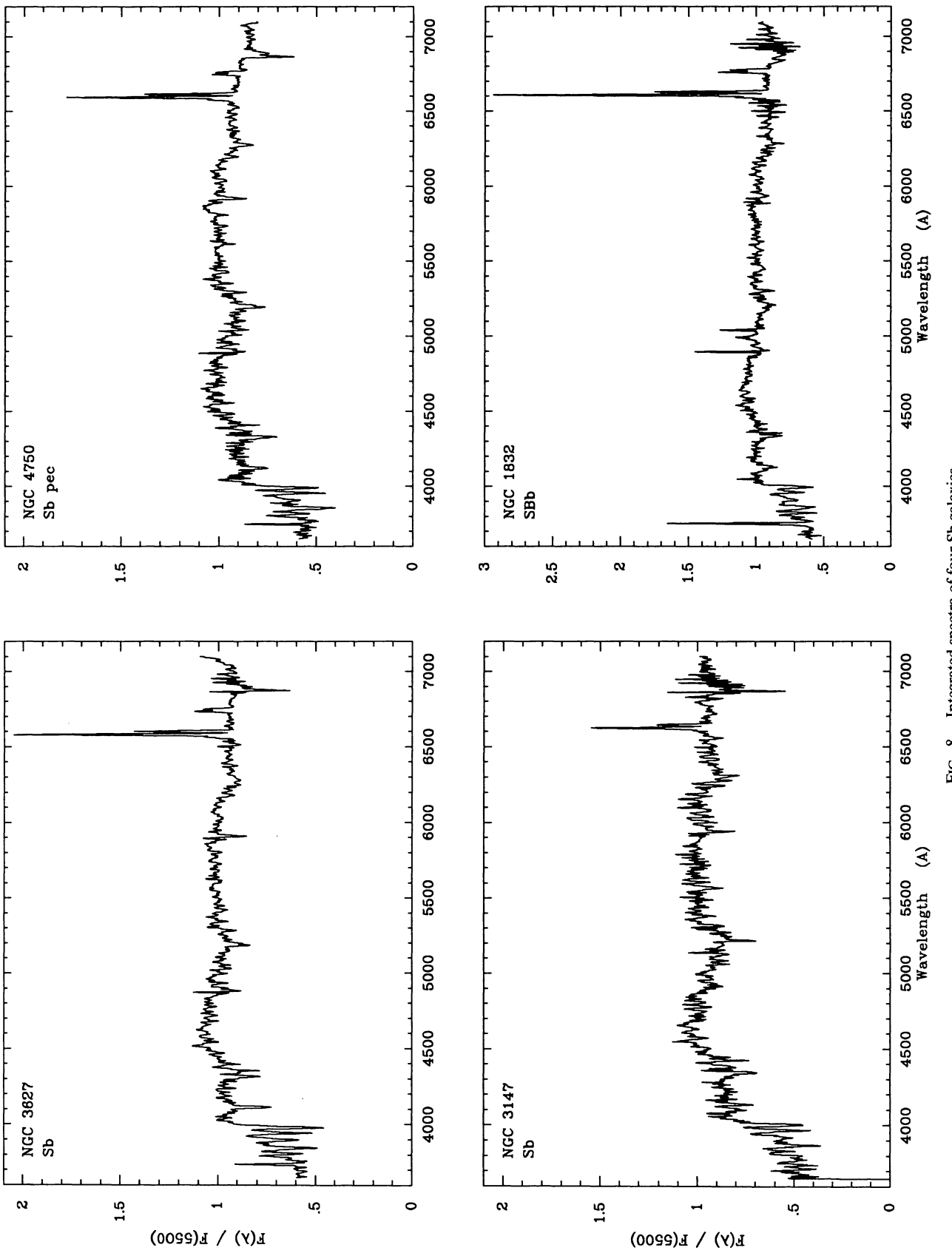

FIG. 8.—Integrated spectra of four Sb galaxies

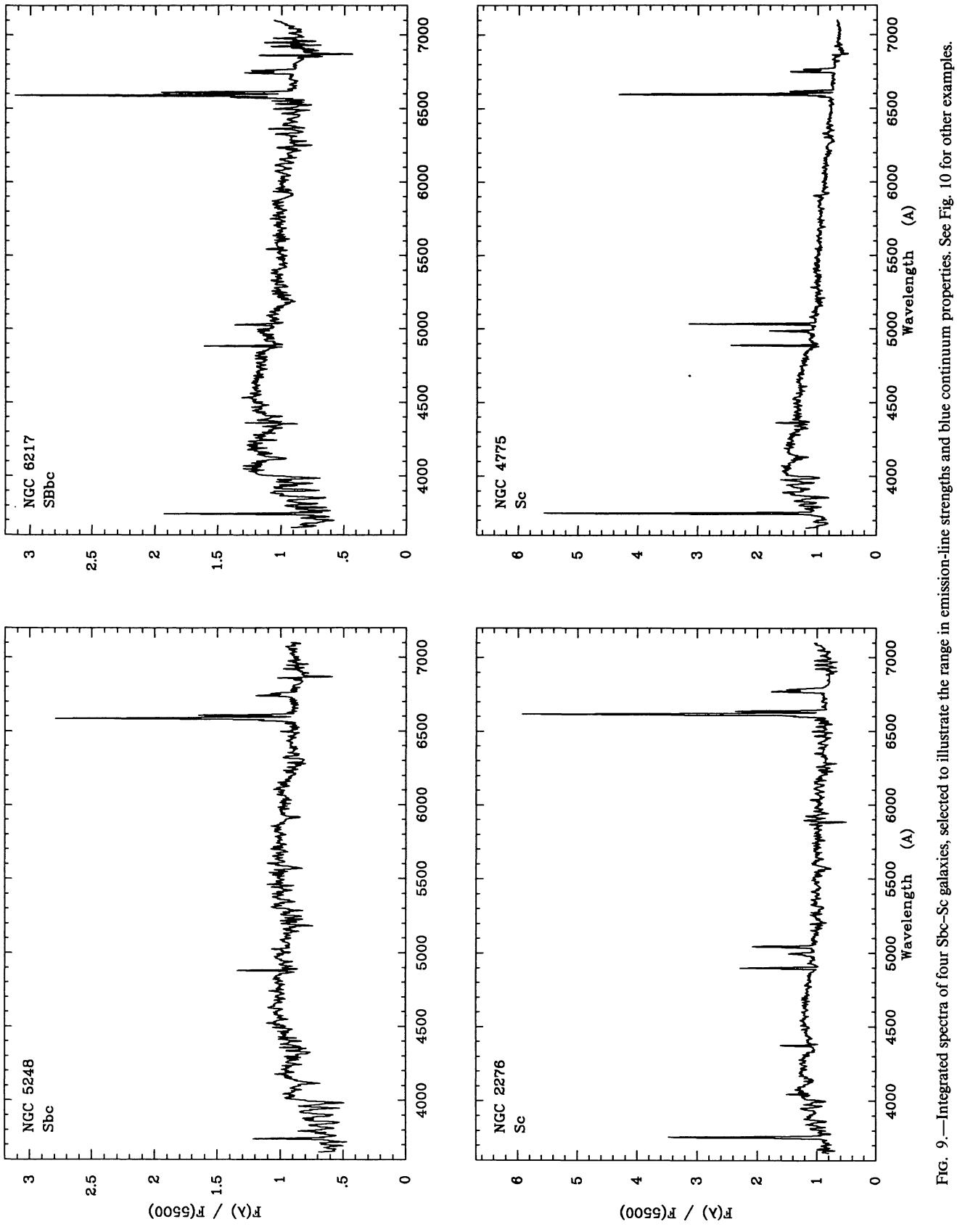

FIG. 9.—Integrated spectra of four Sbc–Sc galaxies, selected to illustrate the range in emission-line strengths and blue continuum properties. See Fig. 10 for other examples.

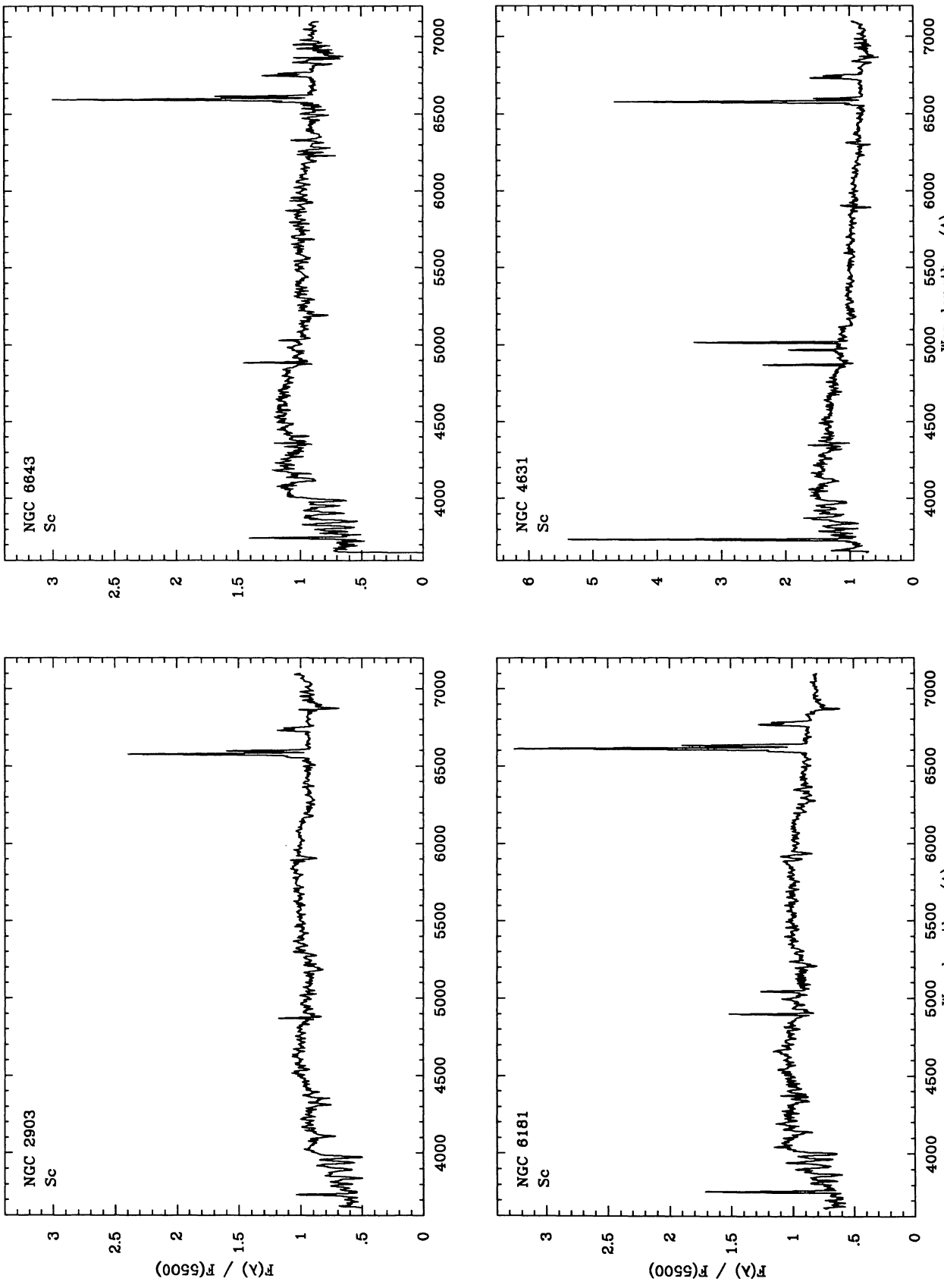

FIG. 10.—Integrated spectra of four Sbc–Sc galaxies, selected to illustrate the range in excitation in the emission-line spectra. See Fig. 9 for other examples.

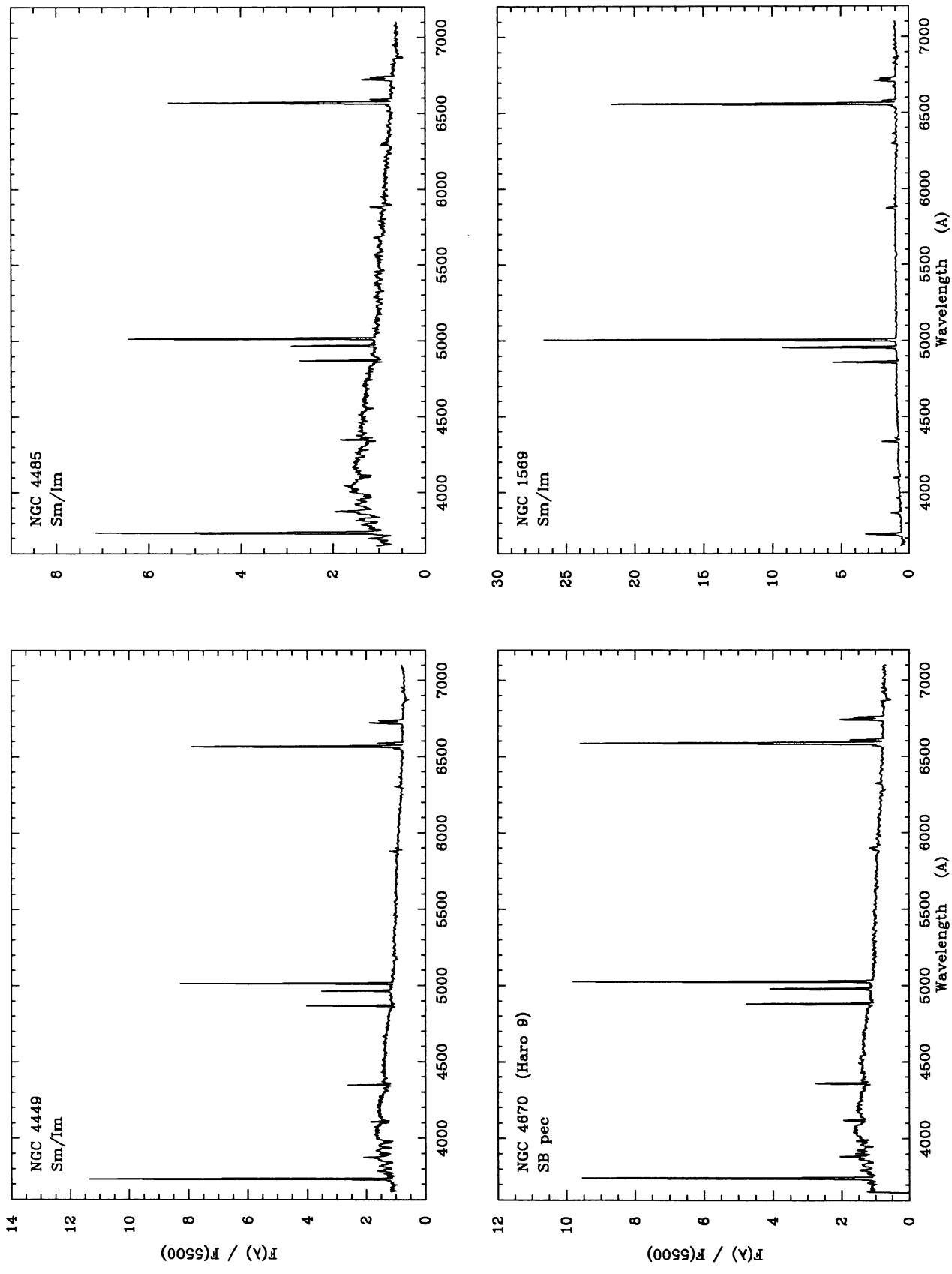

FIG. 11.—Integrated spectra of three Magellanic irregular galaxies (NGC 4449, 4485, 1569), and one peculiar galaxy with a very similar spectrum (NGC 4670).

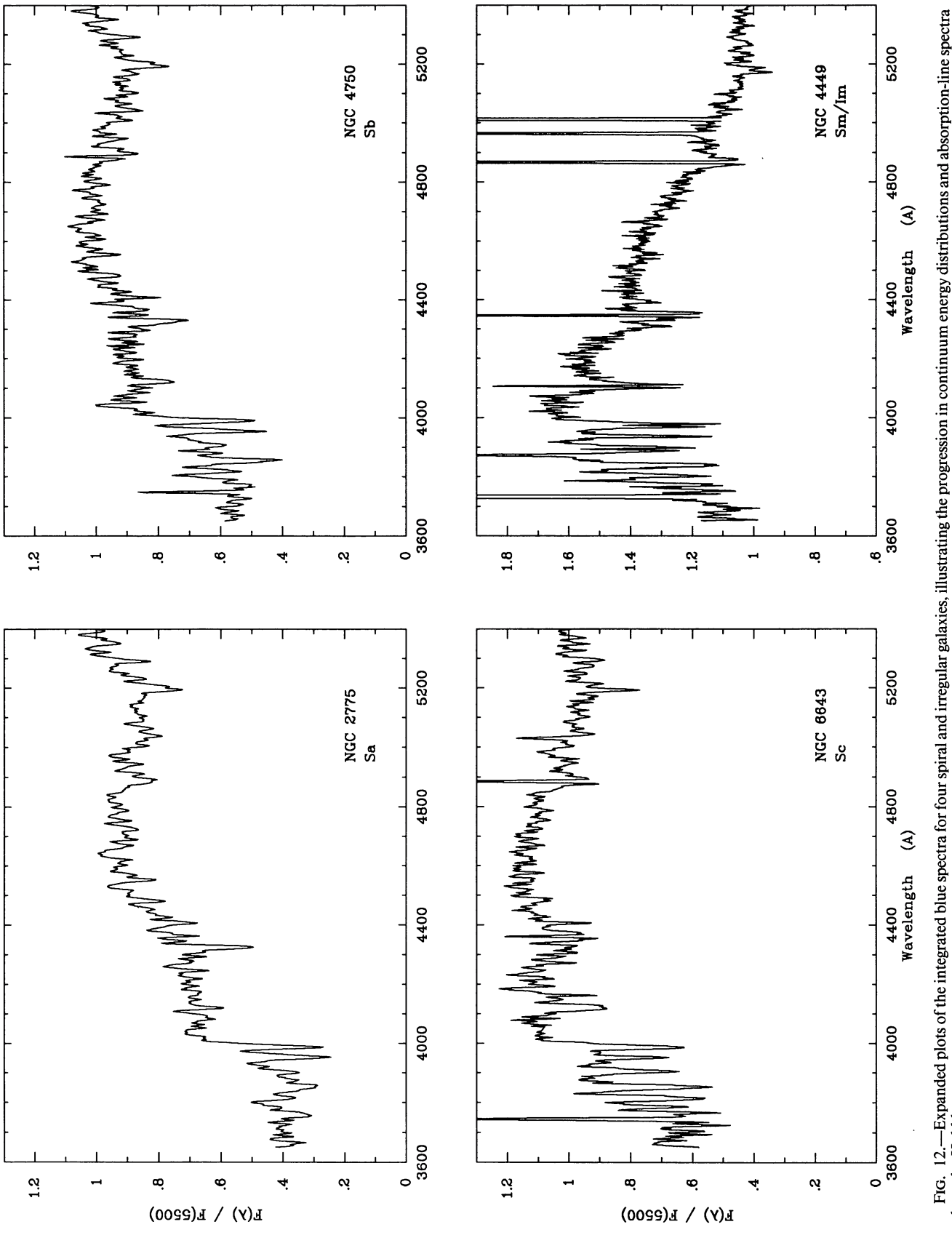

FIG. 12.—Expanded plots of the integrated blue spectra for four spiral and irregular galaxies, illustrating the progression in continuum energy distributions and absorption-line spectra along the Hubble sequence.

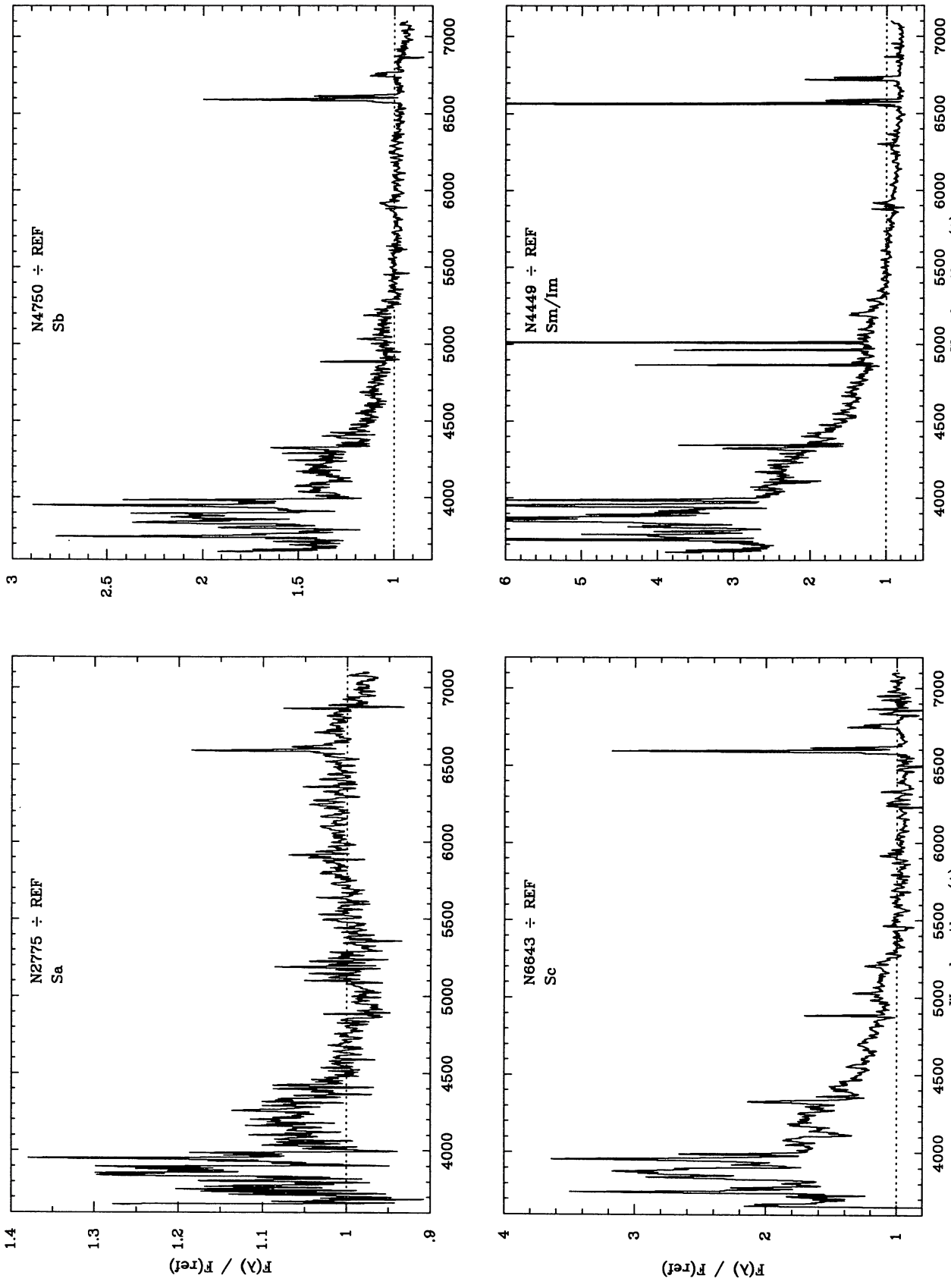

FIG. 13.—For each galaxy the quantity plotted is the observed spectrum (normalized to unity at 5500 Å) divided by the mean spectrum of a set of elliptical and S0 galaxies. The four galaxies are the same as those in Fig. 12.

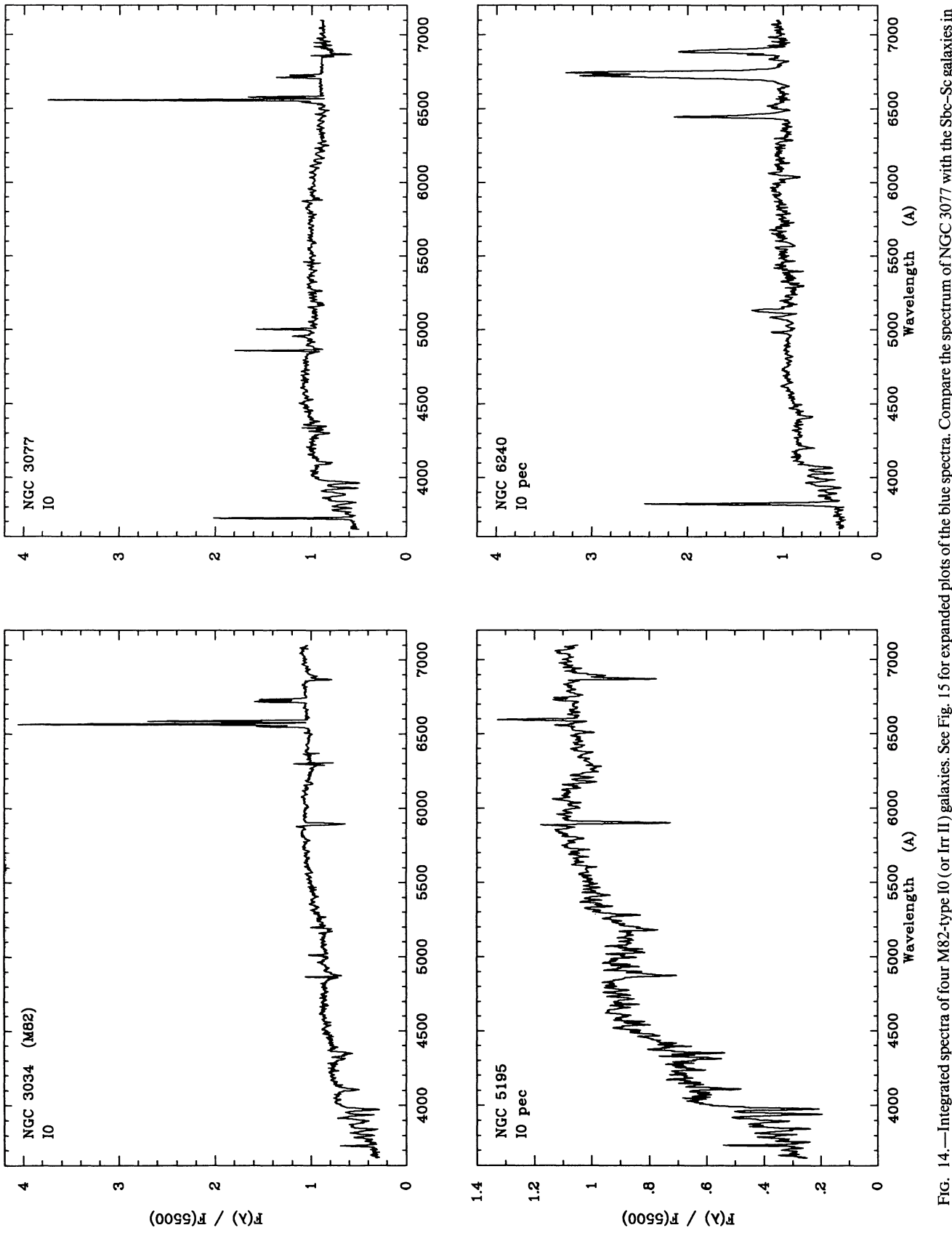

FIG. 14.—Integrated spectra of four M82-type I0 (or Irr II) galaxies. See Fig. 15 for expanded plots of the blue spectra. Compare the spectrum of NGC 3077 with the Sbc–Sc galaxies in Figs. 9–10.

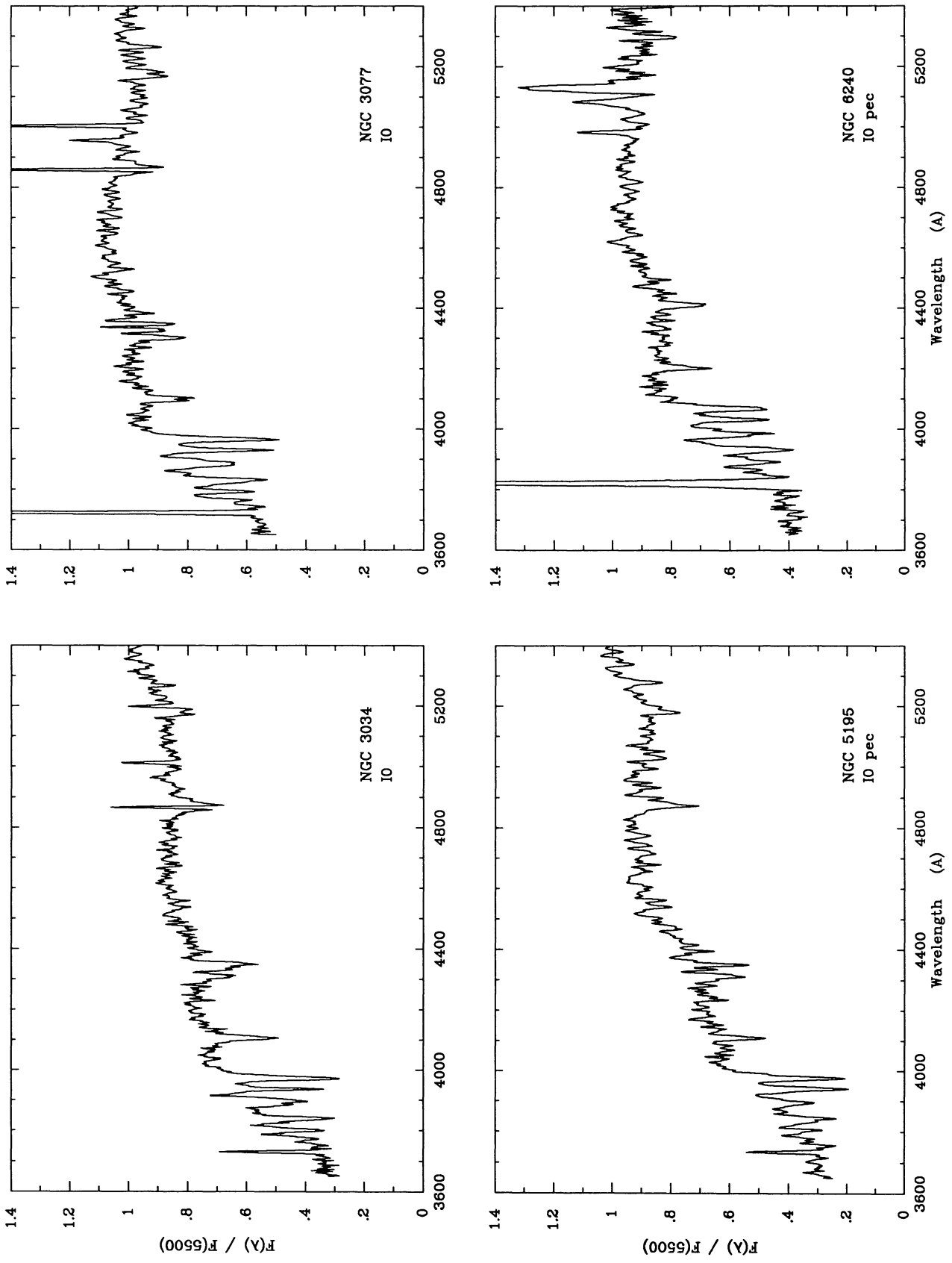

FIG. 15.—Expanded plots of the integrated blue spectra for the four I0 galaxies illustrated in Fig. 14

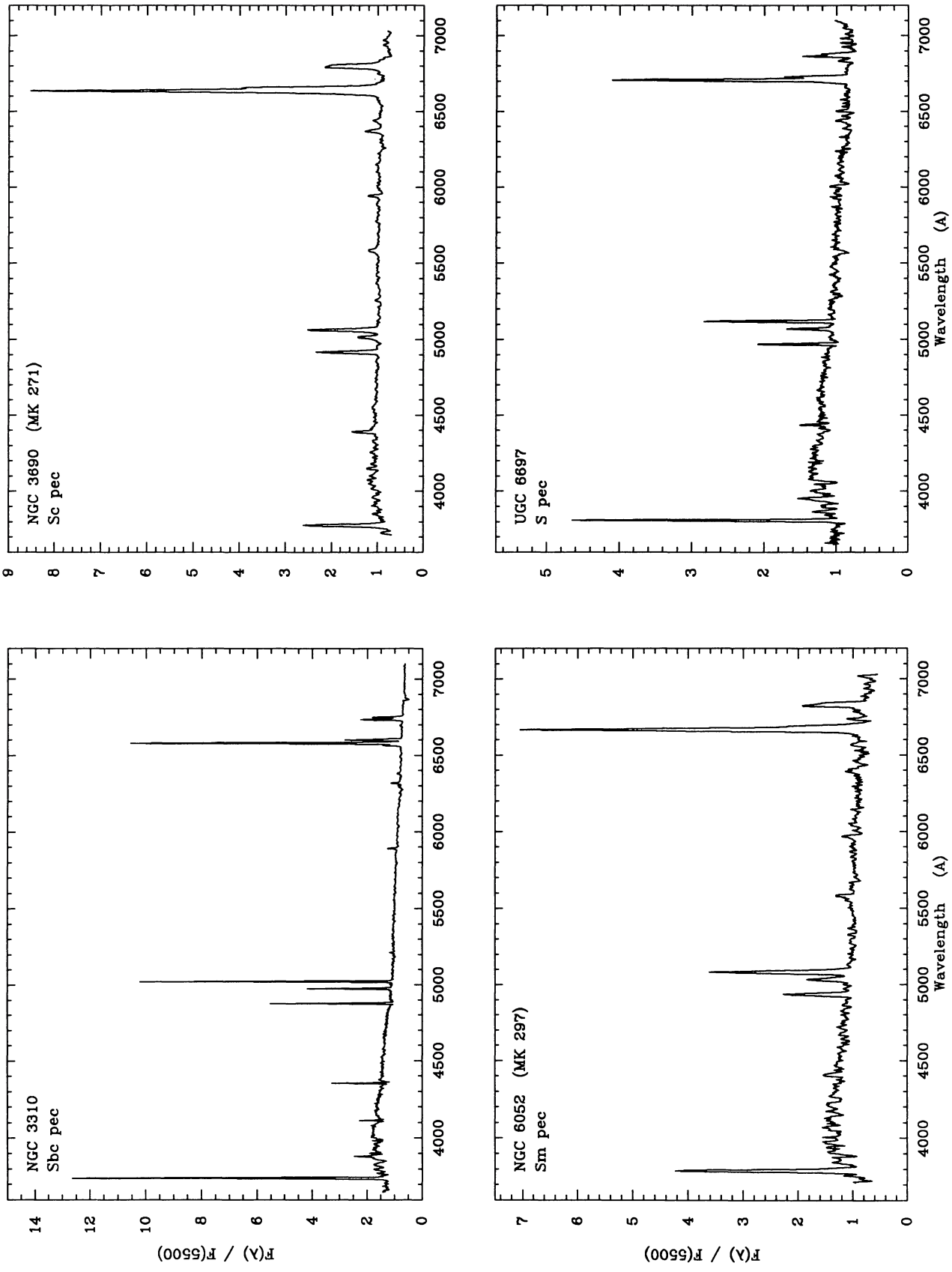

FIG. 16.—Integrated spectra of four spiral and irregular galaxies with global starbursts

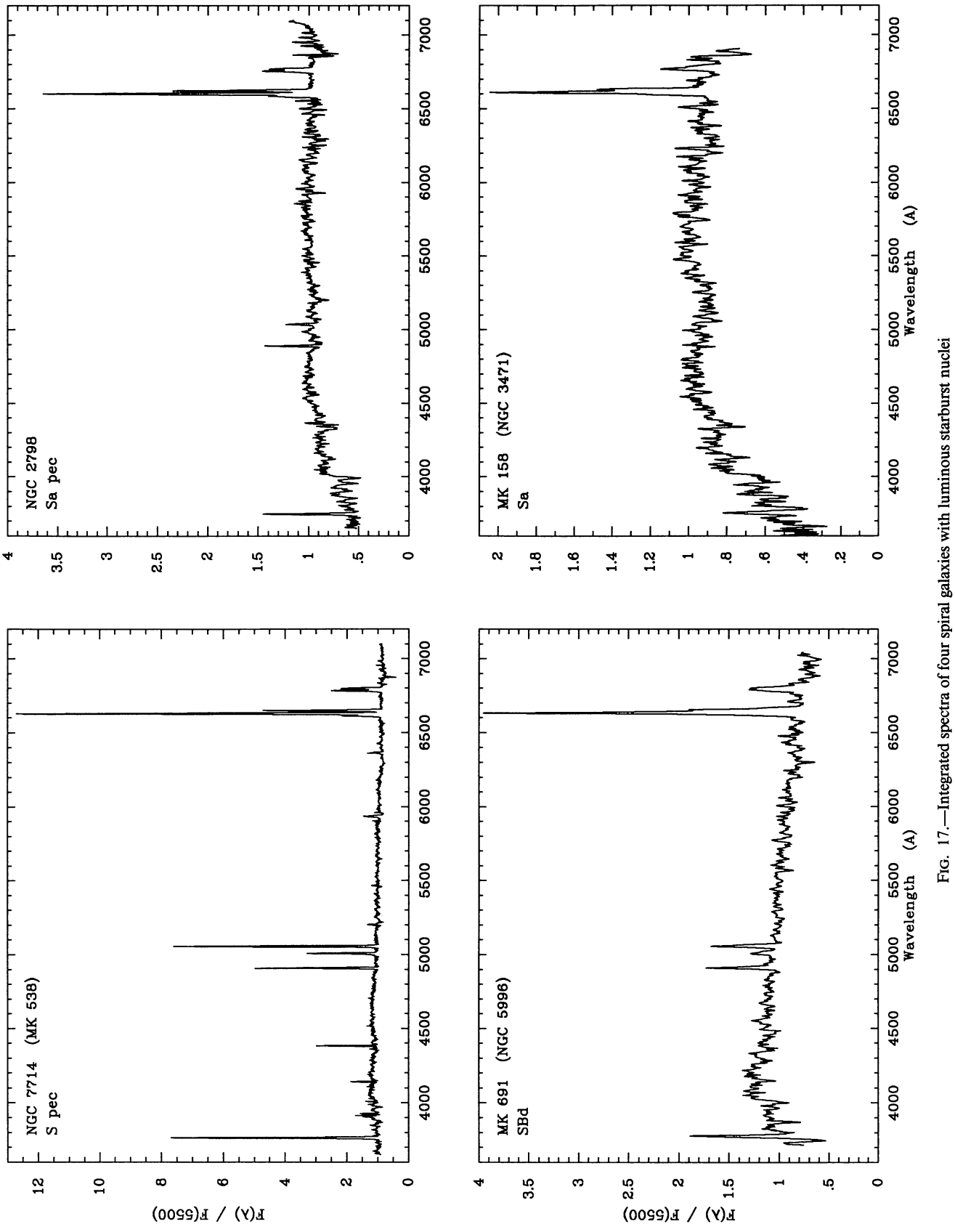

FIG. 17.—Integrated spectra of four spiral galaxies with luminous starburst nuclei

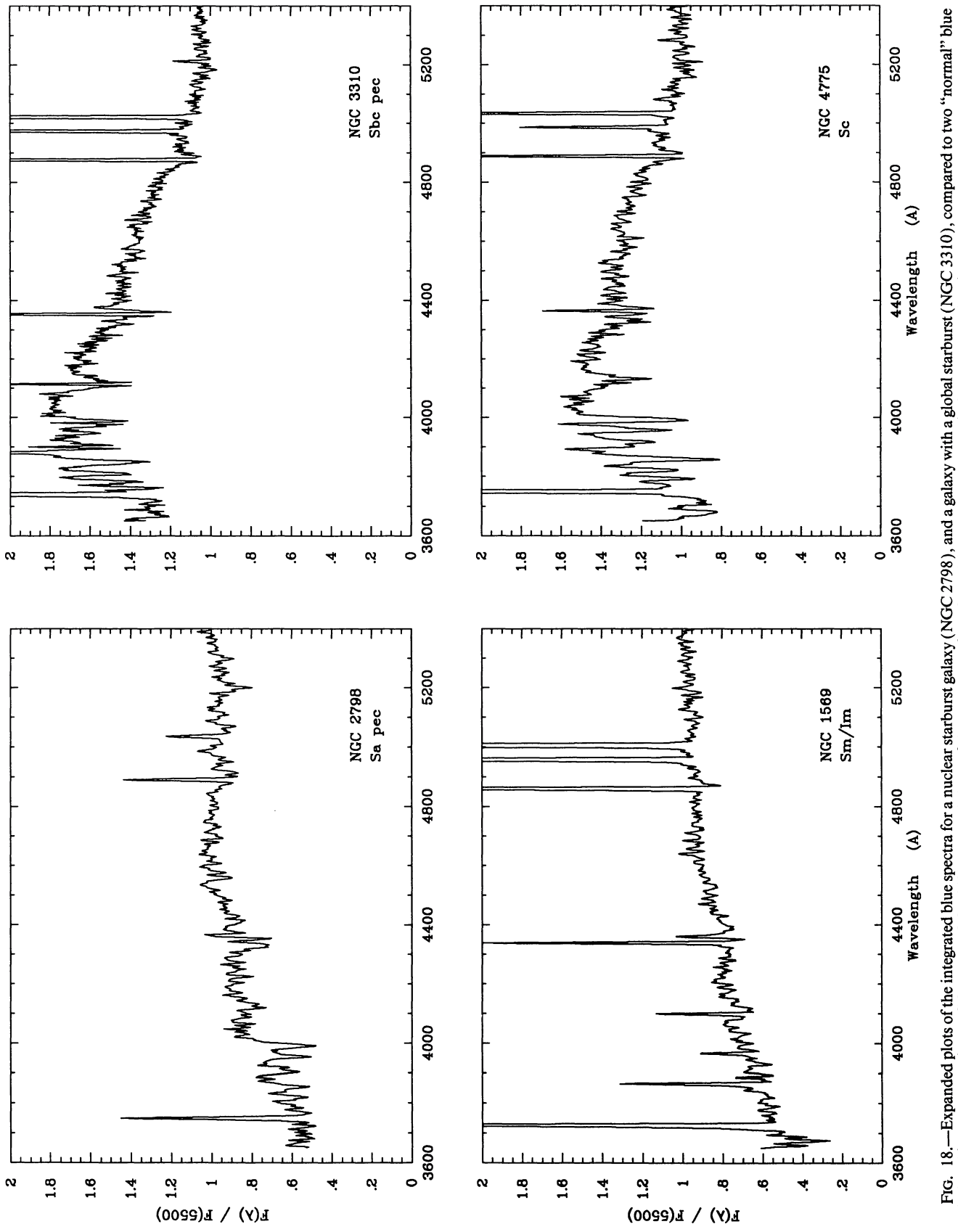

FIG. 18.—Expanded plots of the integrated blue spectra for a nuclear starburst galaxy (NGC 2798), and a galaxy with a global starburst (NGC 3310), compared to two "normal" blue spiral and irregular galaxies (NGC 4775, NGC 1569). The red slope of the spectrum of NGC 1569 is due to high Galactic foreground reddening.

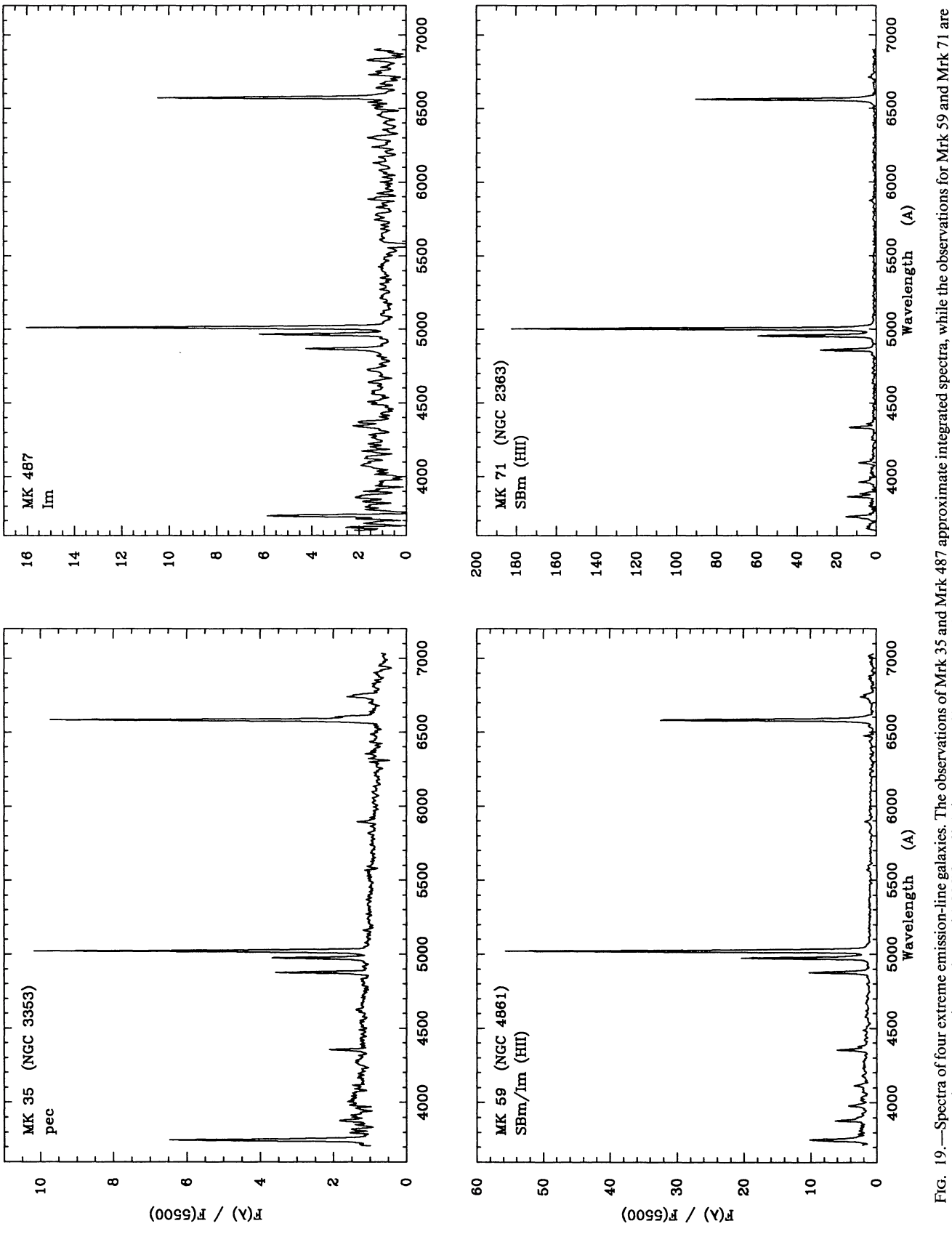

FIG. 19.—Spectra of four extreme emission-line galaxies. The observations of Mrk 35 and Mrk 487 approximate integrated spectra, while the observations for Mrk 59 and Mrk 71 are centered on supergiant H II regions. Along with NGC 1569 (Figs. 11 and 18) these comprise the lowest luminosity and mass galaxies in the atlas.

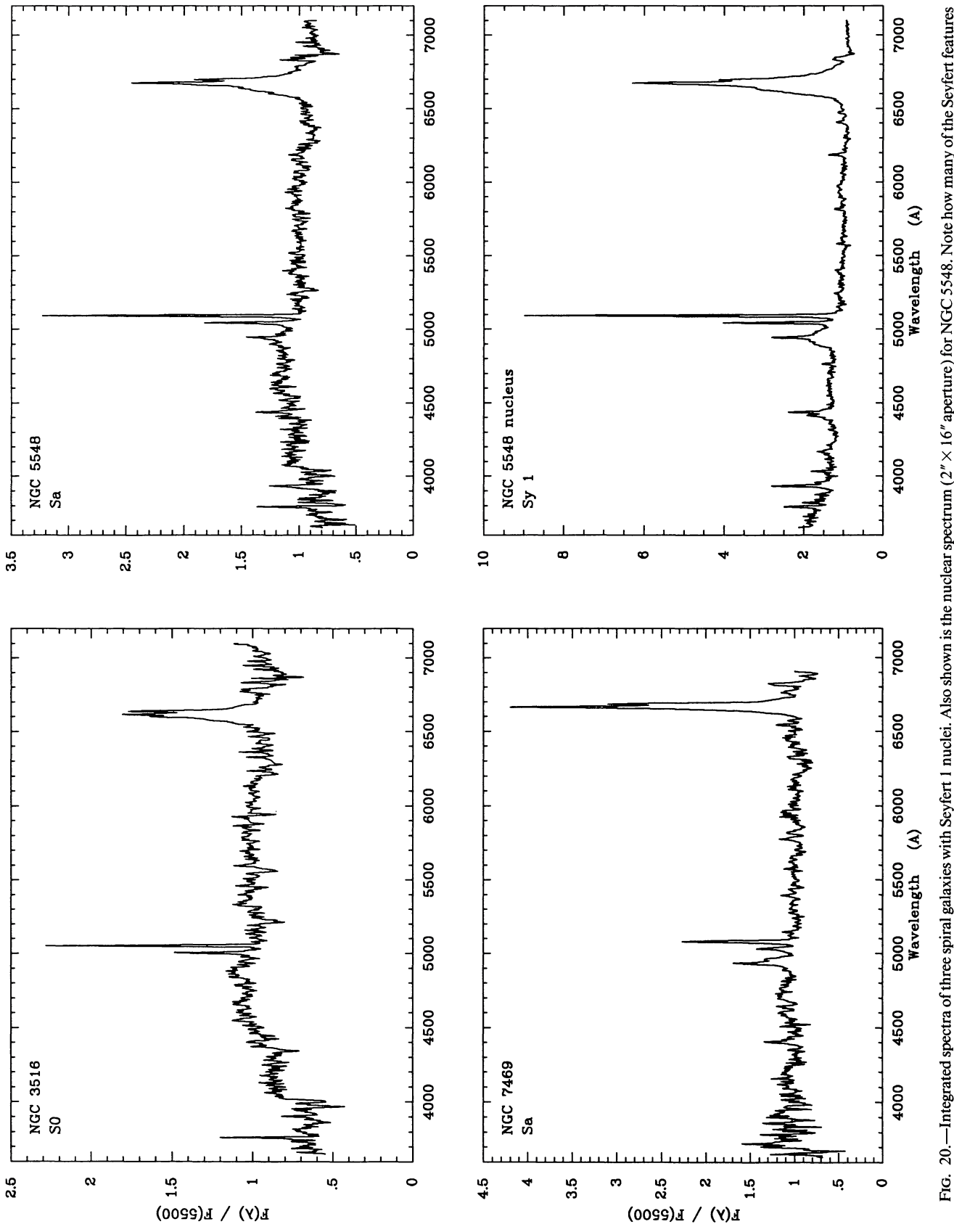

FIG. 20.—Integrated spectra of three spiral galaxies with Seyfert 1 nuclei. Also shown is the nuclear spectrum (2″ × 16″ aperture) for NGC 5548. Note how many of the Seyfert features in the blue become lost in the integrated spectrum of the galaxy.

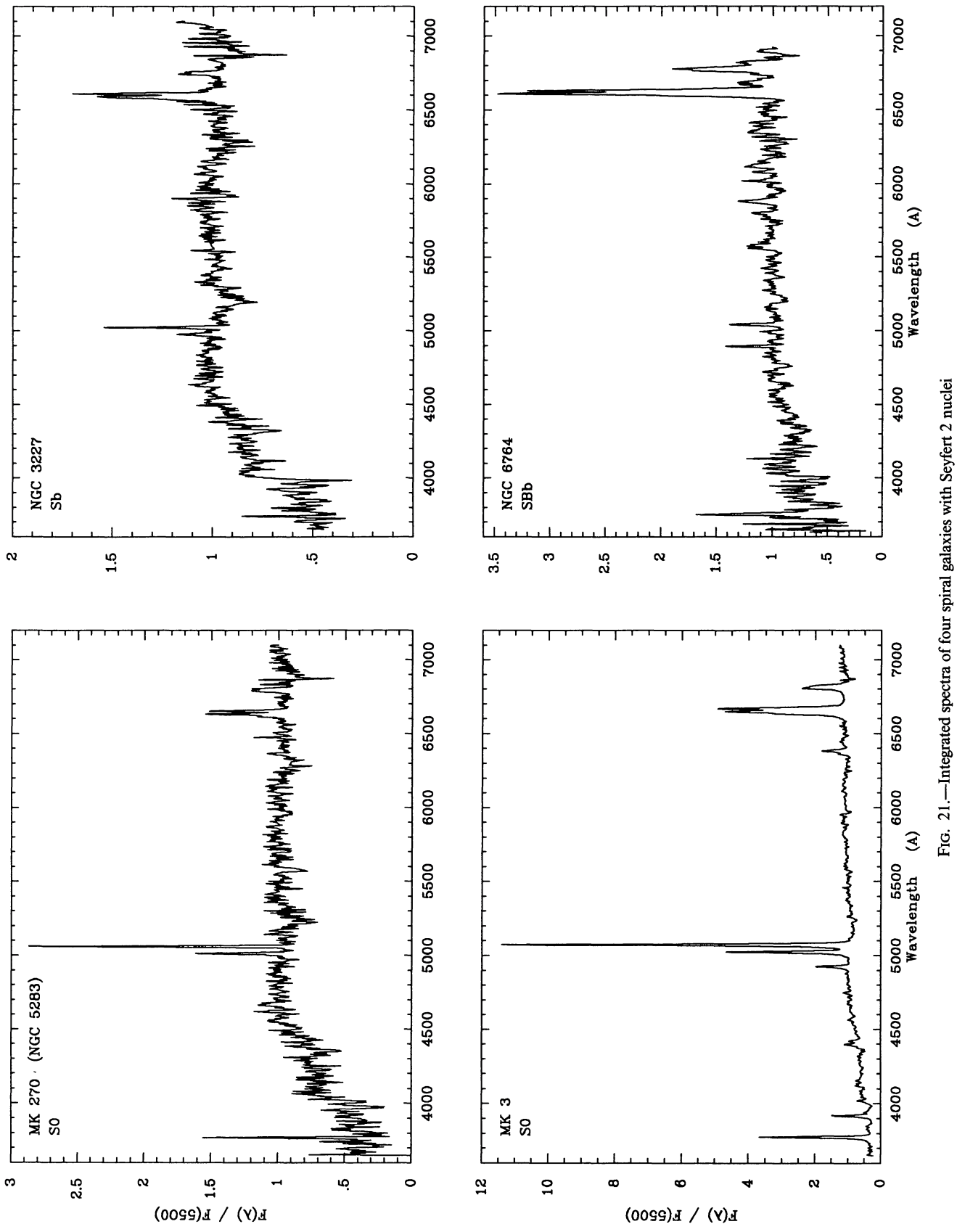

FIG. 21.—Integrated spectra of four spiral galaxies with Seyfert 2 nuclei

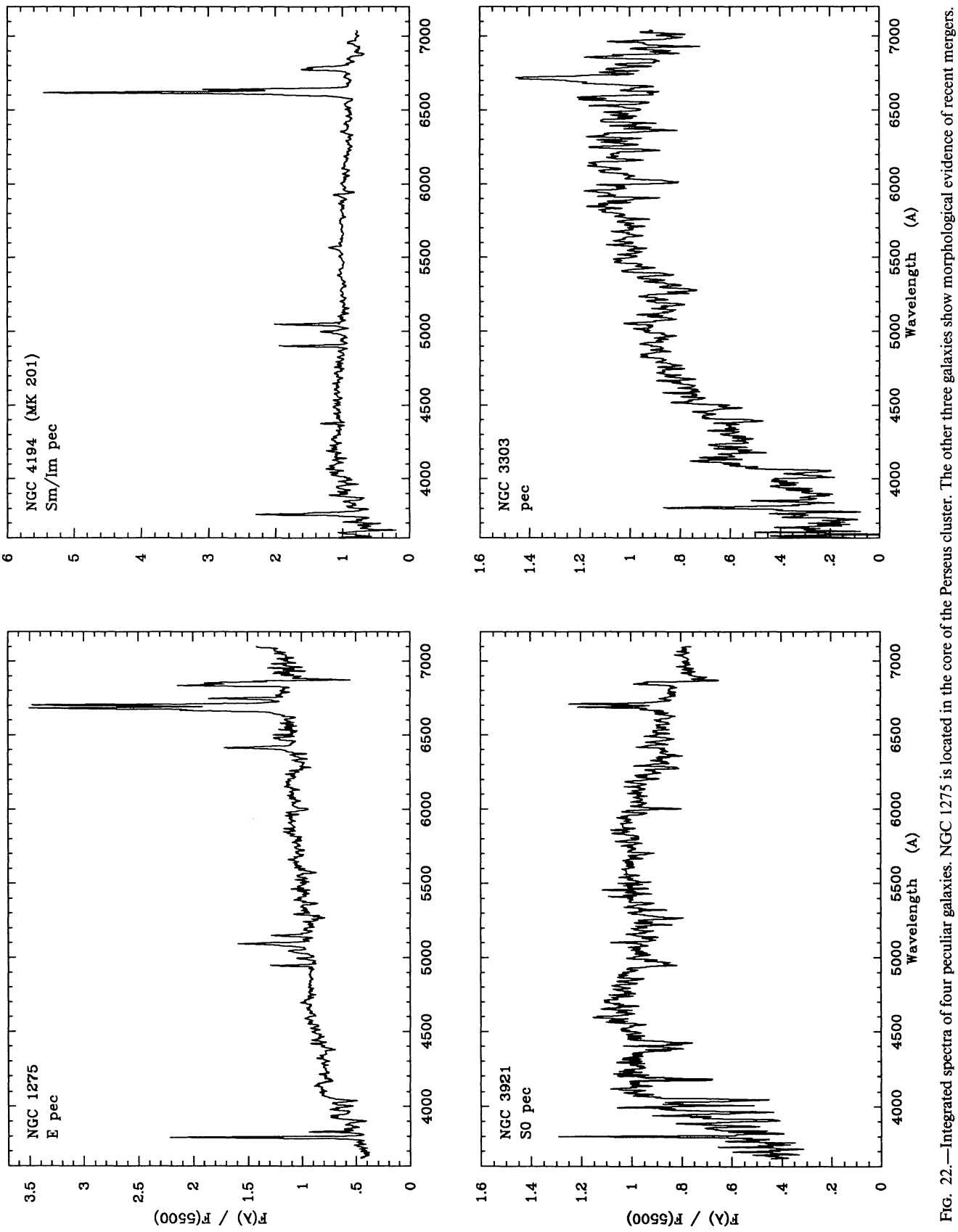

FIG. 22.—Integrated spectra of four peculiar galaxies. NGC 1275 is located in the core of the Perseus cluster. The other three galaxies show morphological evidence of recent mergers.

demonstrates the large range in nebular excitation. Presumably these differences reflect underlying variations in stellar age distribution and mean disk metal abundance, respectively.

The continuum shapes, absorption spectra, and emission line spectra of the Sbc–Sc galaxies are qualitatively different from those of the earlier Hubble types. All of the principal nebular emission lines (Hα, Hβ, [O II], [O III], [N II], [S II]) are apparent in the integrated spectrum, with relative strengths which are characteristic of star-forming H II regions. The stellar continuum and absorption spectrum is composite, with contributions from both the G and K giants and A–F stars, but in the blue, the Balmer spectra of the early-type young stars have become the dominant spectral feature. This differs significantly from the spectral classification of these galaxies on the Yerkes system (Morgan 1958); on the Morgan system, a typical Sc galaxy has a mean spectral type of F to G–K. The difference can be attributed to the fact that the Morgan types were calibrated on the basis of spectra of the near-nuclear regions, where bulge light is much more important. If one were to define a classification for spirals based on their integrated spectra, the spectral types would be systematically earlier (in *stellar* type) than on the Yerkes system.

Figures 9–10 show that within the Sbc–Sc class, there is a large range in the relative contributions of young and old stars, similar to what was seen for the early-type spirals. Once again, these differences are not particularly well correlated with morphological type. Careful examination of the spectra also reveals that continuum shape, absorption spectrum, and line spectrum do not always correlate monotonically. This is probably due in part to variations in reddening among the galaxies, as well as differences in their recent star formation histories.

Figure 10 illustrates the very large range in the nebular excitation among the Sc galaxies. Note in particular the variation in the ratio of [O III] λ5007 to Hβ, and [O II] λ3727 relative to the Balmer lines. The chief cause for these differences (but not the only factor) is a substantial variation in mean H II region abundance among the galaxies. Observations of large numbers of individual H II regions in Sc galaxies show a comparable range in mean excitation (e.g., McCall, Rybski, & Shields 1985; Zaritsky, Elston, & Hill 1990), which these workers attribute to systematic abundance variations, ranging in O/H from a few tenths solar to 1–2 times solar abundance. The range in [O II]/Hβ is somewhat larger than would be expected on the basis of abundance variations alone, however, and other factors, such as reddening variations and contributions from diffuse interstellar gas, may be important. See Paper I for a more detailed discussion.

The sensitivity of the integrated spectrum to mean disk abundance which is apparent in Figure 10 suggests that integrated spectra of distant galaxies should be able to provide some quantitative limits on their chemical composition. This offers the tantalizing prospect of directly probing the evolution in chemical abundances with cosmological lookback time.

3.3.6. *Magellanic Irregular and Spiral Galaxies (Figs. 11, 12, and 18)*

The spectra of these galaxies are completely dominated by young stars and H II regions. This may not be a completely representative sample of irregular galaxies. The high Hα equivalent widths (65–200 Å) and very blue colors indicate that all four galaxies are currently forming stars at a much higher rate than can be sustained over a Hubble time, i.e., we are observing them during an extended star formation burst. For a more representative cross section of Magellanic irregulars, the reader is referred to the extensive series of papers by Gallagher & Hunter (e.g., Hunter & Gallagher 1985, 1986).

At high spectral resolution the nebular emission lines dominate the spectra, making it difficult to discern the stellar absorption features in Figure 10. Expanded plots of the blue spectral region are shown for NGC 4449 and NGC 1569 in Figures 12 and 19, respectively. The absorption spectrum is dominated by Balmer lines, consistent with the classification of these galaxies as A or A–F on the Yerkes system (e.g., Morgan & Mayall 1957).

3.3.7. *Summary of General Trends with Hubble Type*

Before proceeding to a discussion of the peculiar galaxies, it is useful to make a direct comparison of the changes in spectra along the Hubble sequence. The most evident change in spectrum in Figures 5–11 is the increase in the strengths of the nebular emission lines, especially Hα + [N II]. This sensitivity makes the Hα line the best quantitative indicator of the integrated star formation rate in normal galaxies (e.g., Kennicutt 1983, Gallagher, Hunter, & Tutukov 1984). These changes in the nebular spectrum are accompanied by more subtle changes in the continuum and absorption spectra as well. This is perhaps best illustrated in Figure 12, which shows expanded plots of the blue spectral region for examples of Sa, Sb, Sc, and Magellanic irregular galaxies.

A more quantitative depiction of these changes in spectrum with galaxy type is shown in Figure 13. These are not observed spectra, but ratios of normalized spectra, computed as follows. A reference E–S0 galaxy spectrum was created by summing the normalized spectra of NGC 3245, 4262, and 4648 (these were selected because they all have approximately the same redshift), and renormalizing to unity at 5500 Å. Figure 13 then shows the result of dividing the normalized spectra of NGC 2775 (Sa), NGC 4750 (Sb), NGC 6643 (Sc), and NGC 4449 (Im) by the reference spectrum. Taking the difference between the object and reference spectrum (rather than the quotient) yields similar results. Figure 13 provides a direct indication of the relative amounts of excess light over a purely evolved population in each case. Note that most of the choppy structure in the blue is due to slight differences in the positions and profiles of strong lines between the galaxy and template spectra, and hence this structure is not meaningful.

All four galaxies show an excess of younger starlight, with a continuum shape which is characteristic of an A–F star–dominated population. The ratios given on the vertical scales provide a *very rough* indication of the fractional contribution of this younger starlight at various wavelengths. In the Sa galaxy NGC 2775, for instance, only 10%–15% of the blue continuum, at most, is contributed by a blue population, and longward of 4500 Å, the spectral shapes are identical to within the errors of our spectrophotometry. Also notice how clearly the Hα and Hβ emission lines emerge from absorption when divided by the reference spectrum. The Balmer lines appear clearly in the Sb galaxy NGC 4750, and the fraction of blue

starlight rises to of order 20%–50% shortward of 4300 Å. By type Sc, the excess blue component dominates the blue spectrum, contributing over half of the total luminosity in that region.

One should bear in mind that the sample presented here is dominated by bright, high surface brightness galaxies. For practical reasons, very low surface brightness galaxies such as Malin 1 (Impey & Bothun 1989) are not represented. The spectral properties of those objects, and their dependence on Hubble type, could be quite different.

3.4. *Description of Spectra: Peculiar Galaxies*

The remainder of the atlas illustrates spectra of peculiar galaxies of various types. Here I use the term "peculiar" loosely, to encompass morphologically peculiar objects, such as M82-type I0 (Irr II) galaxies, as well as strongly interacting systems, mergers, galaxies with active nuclei, and unusually strong starburst or emission line galaxies. As illustrated in Figures 14–22, these galaxies also exhibit unusual and often unique spectral properties, which may offer important clues to their stellar content and evolutionary histories.

3.4.1. *I0 (Irr II) Galaxies (Figs. 14 and 15)*

Figure 14 shows spectra for four nearby I0 galaxies. The prototype for this class is M82, and all four of the galaxies selected here have very similar optical morphologies, with an amorphous main body, faint filamentary structure, and absorption patches from interstellar dust clouds. Most galaxies of this class are also strong far-infrared sources. Some appear to have been formed as the result of galaxy interactions or mergers (e.g., NGC 5195, 6240).

Despite the morphological similarities between the galaxies in Figure 14, their spectral properties are remarkably heterogeneous. Both M82 and NGC 6240 are dominated by strong Hα + [N II] emission, but their forbidden line spectra are completely different. The nebular line ratios in M82 are characteristic of a combination of normal star-forming regions and shocked gas (note the strong [N II]/Hα and [S II]/Hα), with very high reddening. The spectrum of NGC 6240, while also peculiar, is completely different, with strong broad forbidden lines of [O II] λ3727, [O III] $\lambda\lambda$4959, 5007, [O I] $\lambda\lambda$6300, 6363, [N II] $\lambda\lambda$6548, 6583, and [S II] $\lambda\lambda$6717, 6731. This spectrum is more characteristic of a supernova remnant (multiplied in flux by a factor of billions) than a normal starburst (cf. Figs. 16–18).

NGC 3077 and 5195 represent other extremes. Even though NGC 3077 is morphologically similar to M82 and NGC 5195, its spectrum is indistinguishable from that of a normal spiral (cf. Figs. 9–10). If we were unaware of the appearance of NGC 3077 and were to classify it solely on the basis of its spectrum, it would be mistaken for a normal Sc galaxy! NGC 5195, the irregular companion to M51, shows a highly mixed stellar population, with weak emission lines and very strong Balmer absorption lines superposed upon an evolved underlying spectrum. This is similar to the spectra of blue "E+A" galaxies which are commonly detected at high redshift (e.g., Dressler & Gunn 1983, 1990), except that [N II] and [O II] emission are present in NGC 5195. The spectrum also resembles those observed for the nuclei of many shell elliptical galaxies (Carter et al. 1988).

In contrast to this complete dissimilarity in emission line spectra among these I0 galaxies, the absorption line spectra are surprisingly similar, as illustrated in Figure 15. All of the galaxies show evidence for a composite stellar population, including strong Balmer absorption lines. The most straightforward interpretation of these results is that all four galaxies are experiencing large-scale star formation bursts, but we are observing them at different evolutionary stages. This is consistent with conclusions drawn by Gallagher & Hunter (1987), based on *UBV* and Hα observations of a large sample of similar "amorphous" galaxies. Given the diversity of the spectra of the four galaxies observed here (no two of the spectra are alike), however, it is impossible to draw firm conclusions about the I0 galaxies as a class. More extensive observations, covering a larger sample and properly taking into account the effects of reddening and nonthermal emission, are being made to better understand the nature of these galaxies.

3.4.2. *Starburst and Emission-Line Galaxies (Figs. 16–19)*

Figure 16 shows four examples of galaxies which are undergoing global bursts of star formation. NGC 3690 and NGC 6052 are double systems which are currently undergoing close interactions or mergers. The spectra were taken with the IRS, and the apparent line broadening relative to the other galaxies is entirely instrumental. NGC 3310 is a single Sbc galaxy, but the presence of a nucleus which is offset from the dynamical center of the galaxy and tidal debris at large radii have led Balick & Heckman (1981) to classify the system as an evolved merger. UGC 6697 is located in the Abell 1367 cluster and appears to be undergoing a strong interaction with the local intergalactic medium (Gavazzi & Jaffe 1987).

These galaxies possess some of the strongest emission lines in the survey, with equivalent widths of Hα + [N II] ranging from 77 to 234 Å (Paper I), 3–10 times higher than in an average Sb or Sc galaxy. The stellar continua also resemble late-type, active star-forming galaxies. The principal difference between these luminous starburst galaxies and the Magellanic irregulars shown in Figure 11 is a somewhat lower mean excitation, which is consistent with the fact that these tend to be more massive (and probably metal-rich) galaxies.

Figure 17 shows spectra for four *nuclear* starburst galaxies, as defined by Balzano (1983). These differ from the galaxies in Figures 16 and 19, in that most of the starburst activity is concentrated in an H II region–like nucleus, and the parent galaxies are often of earlier Hubble type. The emission line spectra of NGC 7714, NGC 2798, and Mrk 691 closely resemble those in Figure 16; it would be difficult to distinguish between global and nuclear starbursts if only the integrated spectra were available. A closer comparison of the blue continua of these galaxies, shown in Figure 18, reveals some differences. In NGC 2798, for example, which consists of a very luminous starburst nucleus within a relatively quiescent Sa galaxy, the absorption spectrum shows a highly composite nature, with Balmer lines from the starburst superposed on a red, evolved spectrum of the Sa galaxy. This is uncharacteristic of galaxies with global starbursts (e.g., NGC 3310 in Fig. 18), where the young stellar population dominates the entire spectrum. The

starburst nuclei also tend to show lower nebular excitation, which probably reflects the higher mean metal abundances in the inner regions of most spirals, but this is not always the case.

One of the nuclear starburst galaxies in Figure 17, Mrk 158 (NGC 3471) shows a very different integrated spectrum, with very strong Hα and [N II] emission, but only weak emission lines in the blue, and a relatively red continuum. This object, which was identified as a starburst galaxy on the basis of its optical morphology and strong Hα emission, would not be identified as a starburst at all if only its blue spectrum were available. This provides another illustration of how difficult it can be to classify a distant galaxy based on its blue spectrum alone.

Finally, Figure 19 shows four examples of extreme emission-line galaxies. In these cases the equivalent widths of the Hα + [N II] emission lines range from 160 to over 1000 Å! All four of the spectra were obtained with the IRS using 45″ apertures. Two of the observations, for Mrk 35 and Mrk 487, are essentially integrated measurements. Mrk 59 and Mrk 71 are large H II/OB complexes within the nearby Magellanic irregular galaxies NGC 4861 and NGC 2363, respectively, and hence their spectra are not strictly integrated measurements of their respective galaxies. However, if either galaxy were observed from a large distance, it is likely that their integrated spectra would be dominated by the giant H II regions. The galaxies in Figure 19 possess a large range in total luminosities and metal abundances, and this is seen as a very large range in nebular excitation. The O/H abundances in Mrk 59 and Mrk 71 are approximately 0.1 solar (Garnett 1989). Consequently those objects provide an indication of how the spectrum of a truly primeval galaxy might appear.

3.4.3. *Seyfert Galaxies (Figs. 20 and 21)*

The integrated spectra of galaxies with active nuclei, especially Seyfert galaxies, are of particular relevance to spectroscopic surveys of distant galaxies, because such galaxies may be preferentially detected in such surveys, and often their integrated spectra are difficult to distinguish from those of starbursting emission line galaxies.

Figure 20 shows spectra of three Seyfert 1 galaxies, along with the nuclear spectrum of one of the galaxies (NGC 5548). When the full optical spectrum is available, these galaxies are easily identified by the presence of very broad Hα emission. The separation is less straightforward, however, if only the blue spectral region is available, as is often the case in surveys of distant galaxies. Unless the nucleus is much brighter than the surrounding galaxy, the high-velocity wings of the Balmer lines blend into the continuum of the parent galaxy (e.g., NGC 3516 and NGC 5548 in Fig. 20). Paper I discusses quantitative means of identifying the Seyfert galaxies in this situation. Although the strong, narrow forbidden lines in the Seyfert galaxies closely resemble those seen in starburst galaxies, the underlying stellar continuum, often dominated by the early-type parent galaxy, is quite distinct from that in a starburst galaxy (compare with Figs. 16–18), and this often provides an effective means of separating the two types of objects.

Figure 21 shows spectra for four nearby Seyfert 2 galaxies. In this case there are no broad Balmer lines to provide an unambiguous signature of an active nucleus, but as in the case of the Seyfert 1 galaxies, the mismatch between a strong, high-excitation emission-line spectrum and a relatively red, evolved continuum is the best indication that the emission arises from an active nucleus, rather than a starburst. Note the presence of a high-excitation emission-line spectrum is *not* by itself sufficient evidence to classify the spectrum as a Seyfert galaxy. In many Sc–Irr and starburst galaxies strong stellar Balmer absorption will virtually obliterate the Hβ emission line, especially at low spectral evolution, and the resulting high excitation spectrum will be virtually indistinguishable from that of a Seyfert 2 galaxy.

3.4.4. *Peculiar Galaxies, Mergers (Fig. 22)*

The four final galaxies, shown in Figure 22, are among the most peculiar objects in the survey, and this peculiarity extends to their integrated spectra as well. A common trait among these objects is evidence of a recent merger event, either with another galaxy (NGC 3303, 3921, 4194), or with a large amount of intergalactic gas (NGC 1275). The I0 galaxy NGC 6240, with the bizarre spectrum shown in Figures 14–15, also falls in this category.

The integrated spectrum of NGC 1275 is the most peculiar in the survey. The two well-known velocity systems in the ionized gas are clearly resolved here. Much of the emission in this galaxies is produced by a cooling flow in the core of the Perseus cluster (Heckman et al. 1989), and this spectrum provides some indication of how a distant cooling flow might appear.

The other three galaxies in Figure 22 show different examples of how galactic mergers can alter the stellar populations. The spectrum of NGC 4194 (Mrk 201) is dominated by a starburst and closely resembles the other emission line galaxies in Figures 16–18. NGC 3921 shows a mixed population, with extraordinarily strong Balmer absorption lines. This is another nearby analog to the "E+A" galaxies which are frequently observed at high redshift. The E+A galaxies have been postulated to be the relics of mergers at earlier cosmological epochs (e.g., Dressler & Gunn 1983), and the spectroscopic resemblence between those galaxies and the nearby examples of mergers offers some circumstantial support to this hypothesis. The spectrum of NGC 3303 is of poorer quality, but it shows evidence of some of the same features, including Balmer absorption (but much weaker) superposed on an older stellar spectrum, but with extremely strong [O II] emission. As was the case with the I0 galaxies discussed earlier, the mergers show such a wide range in spectral properties that it is impossible to draw any general conclusions about the spectral properties of the class. Observations of a much larger sample are in progress, and they show an even larger diversity in spectral properties (C. T. Liu & R. C. Kennicutt, in preparation).

3.5. *Availability of the Atlas in Digital Form*

For many applications, the reduced plots shown in this paper will be difficult to use. A digital version of the data is available upon request from the Astronomical Data Center (ADC). The data may be obtained in machine-readable form, either on magnetic tape or possibly via transmission over an electronic network. Individuals should complete and submit the form published in the latest issue of the *Astronomical Data Center Bulletin,* or transmit the information on the

form to the ADC by telephone to (301) 286-8310, or electronic mail to TEADC@SCFVM (BITnet), TEADC@SCFVM.GSFC.NASA.GOV (Internet), or NSSDCA::ADCREQUEST (NSI-DECnet). Note that the stellar library of Jacoby et al. (1984) is also available from the ADC.

I wish to express my thanks to Dennis Means, Gary Rosenbaum, and Vic Hansen, for capable and patient assistance with the unorthodox drift-scanning observations, and to Joni Johnson and Dimitri Klebe for assistance with the KPNO observations. I am also grateful to Richard Elston, Hans Rix, Tim Heckman, Nelson Caldwell, and the referee for useful comments and suggestions. George Jacoby generously supplied the data which appear in Figure 4. This research was supported by NSF grants AST-8613257 to the University of Minnesota, and AST-8996123 and AST-9090150 to the University of Arizona.

REFERENCES

Balick, B., & Heckman, T. 1981, A&A, 96, 271
Balzano, V. A. 1983, ApJ, 268, 602
Barnes, J. V., Massey, P., & Carder, E. 1986, IRS Instrument Manual, Kitt Peak National Observatory
Caldwell, N., Kennicutt, R., Phillips, A. C., & Schommer, R. A. 1991, ApJ, 370, 526
Carter, D., Prieur, J. L., Wilkinson, A., Sparks, W. B., & Malin, D. F. 1988, MNRAS, 235, 813
de Vaucouleurs, G., de Vaucouleurs, G., & Corwin, H. G. 1976, Second Reference Catalog of Bright Galaxies (Austin: Univ. of Texas Press)
Dressler, A., & Gunn, J. E. 1982, ApJ, 263, 533
———. 1983, ApJ, 270, 7
———. 1990, in Evolution of the Universe of Galaxies, ed. R. G. Kron (ASP Conf. Ser., 10), 200
Ellis, R. S. 1990, in Evolution of the Universe of Galaxies, ed. R. G. Kron (ASP Conf. Ser., 10), 248
Gallagher, J. S., Bushouse, H., & Hunter, D. A. 1989, AJ, 97, 700
Gallagher, J. S., & Hunter, D. A. 1987, AJ, 94, 43
Gallagher, J. S., Hunter, D. A., & Tutukov, A. V. 1984, ApJ, 284, 544
Garnett, D. R. 1989, ApJ, 345, 282
Gavazzi, G., & Jaffe, W. 1987, A&A, 186, L1
Gregg, M. D. 1989, ApJ, 337, 45
Heckman, T. M., Baum, S. A., van Breugel, W. J. M., & McCarthy, P. 1989, ApJ, 338, 48
Hubble, E. 1926, ApJ, 64, 326
Huchra, J. P. 1977, ApJS, 35, 171
Humason, M. L. 1931, ApJ, 74, 35
———. 1936, ApJ, 83, 18
Hunter, D. A., & Gallagher, J. S. 1985, ApJS, 58, 533
———. 1986, PASP, 98, 5
Impey, C., & Bothun, G. 1989, ApJ, 341, 89
Jacoby, G. H., Hunter, D. A., & Christian, C. A. 1984, ApJS, 56, 257
Kennicutt, R. C. 1983, ApJ, 272, 54
———. 1992, ApJ, in press
Kormendy, J., & Djorgovski, S. 1989, ARA&A, 27, 235
Massey, P., Strobel, K., Barnes, J. V., & Anderson, E. 1988, ApJ, 328, 315
McCall, M. L., Rybski, P. M., & Shields, G. A. 1985, ApJS, 57, 1
Morgan, W. W. 1958, PASP, 70, 364
———. 1959, PASP, 71, 92
Morgan, W. W., & Mayall, N. U. 1957, PASP, 69, 291
Morgan, W. W., & Osterbrock, D. E. 1969, AJ, 74, 515
Osterbrock, D. E. 1960, ApJ, 132, 325
Sandage, A., & Tammann, G. A. 1981, A Revised Shapley-Ames Catalog of Bright Galaxies (Washington, DC: Carnegie Institution of Washington)
Schild, R., & Oke, J. B. 1971, ApJ, 169, 209
Silva, D. R. 1991, Ph.D. thesis, Univ. Michigan
Wells, D. G. 1972, Ph.D. thesis, Univ. Texas
Whitford, A. E. 1971, ApJ, 169, 215
Woolf, N. J. 1982, ARA&A, 20, 367
Zaritsky, D., Elston, R., & Hill, J. M. 1990, AJ, 99, 1108